Title: PSD-95 in dorsal CA1 contributes to the persistence of fear memory

Authors: Magdalena Ziółkowska[&,1], Malgorzata Borczyk[&,1,2], Agata Nowacka[1], Maria Nalberczak-Skóra[1], Małgorzata Alicja Śliwińska[1,3], Magdalena Robacha[1], Kacper Łukasiewicz[1], Anna Cały[1], Edyta Skonieczna[1], Kamil F. Tomaszewski[1], Tomasz Wójtowicz[4], Jakub Włodarczyk[4], Tytus Bernaś[3,5], Ahmad Salamian[1] and Kasia Radwanska[1*].

[1]Laboratory of Molecular Basis of Behavior, the Nencki Institute of Experimental Biology of Polish Academy of Sciences.

[2]Department Molecular Neuropharmacology, Maj Institute of Pharmacology of Polish of Academy of Sciences, Warsaw, Poland.

[3]Laboratory of Imaging Tissue Structure and Function, The Nencki Institute of Experimental Biology of Polish Academy of Sciences, Warsaw, Poland.

[4]Laboratory of Cell Biophysics, the Nencki Institute of Experimental Biology of Polish Academy of Sciences.

[5]Department of Anatomy and Neurology, VCU School of Medicine, 1101 East Marshall Street, Richmond, Virginia 23298.

[&]equal contribution.

***Corresponding author**: Kasia Radwanska, Ph.D., Laboratory of Molecular Basis of Behavior, Nencki Institute of Experimental Biology of Polish Academy of Sciences, ul. L. Pasteura 3, Warsaw 02-093, Poland; e-mail: k.radwanska@nencki.edu.pl; tel: +48501736942.

Key words**:** PSD-95, contextual fear memory, extinction, dorsal CA1, synaptic plasticity

Number of pages: 35
Number of figures, tables, multimedia and 3D models (separately)
Figures (6), tables (0), multimedia and 3D models (0), supplementary figures (6)
Number of words for Abstract, Introduction, and Discussion (separately)
Abstract (135), Introduction (373), Discussion (893)

ABSTRACT

The ability to update and extinguish fearful memories is essential for survival. Accumulating data indicate that the dorsal CA1 area (dCA1) contributes to this process. However, the cellular and molecular basis of fear memory updating remains poorly understood. Postsynaptic density protein 95 (PSD-95) regulates the structure and function of glutamatergic synapses. Here, we investigated the role of dCA1 PSD-95-driven synaptic plasticity in contextual fear extinction. Using dCA1-targeted genetic manipulations *in vivo* combined with PSD-95 immunostaining and 3D electron microscopy *ex vivo*, we demonstrate that phosphorylation of PSD-95 at serine 73 PSD-95(S73) is necessary for contextual fear extinction-induced expression of PSD-95 and remodeling of glutamatergic synapses. Surprisingly, PSD-95 phosphorylation is not necessary for fear memory formation or early extinction but is required for updating a partly extinguished fear memory, affecting its persistence. Using a chemogenetic manipulation, we confirm that updating of the partly extinguished fear requires PSD-95 expression and dCA1 activity during a prior extinction session. Overall, our data indicate that dCA1 synapses are remodeled upon the extinction of contextual fear memories; this process relies on PSD-95(S73) phosphorylation and enables future updating of a partly extinguished contextual fear memory. These findings show how the hippocampus may contribute to the persistence of fear memories.

INTRODUCTION

The ability to form, store, and update fearful memories is essential for animal survival. In mammals, the formation and updating of such memories involve the hippocampus (Baldi and Bucherelli, 2015; Frankland and Bontempi, 2005; Neves et al., 2008; Strange et al., 2014). In particular, the formation of contextual fear memories strengthens Schaffer collaterals in the dorsal CA1 area (dCA1) through NMDA receptor-dependent Hebbian forms of synaptic plasticity (Abraham et al., 2019; Bliss and Collingridge, 1993; Morris et al., 2003) linked with growth and addition of new dendritic spines (harboring glutamatergic synapses) (Aziz et al., 2019; Mahmmoud et al., 2015; Radwanska et al., 2011; Restivo et al., 2009). Similarly, contextual fear extinction induces functional, structural, and molecular alterations of dCA1 synapses (Garín-Aguilar et al., 2012; Schuette et al., 2020; Stansley et al., 2018). While synaptic plasticity in the dCA1 in contextual fear memory formation has been recently questioned (Bannerman et al., 2014), its role in contextual fear memory extinction is mostly unknown. Understanding the molecular and cellular mechanisms that underlie fear extinction memory is crucial to develop new therapeutic approaches to alleviate persistent and unmalleable fear.

PSD-95 is the major scaffolding protein of a glutamatergic synapse (Cheng, 2006), affecting its stability and maturation (Ehrlich et al., 2007; Steiner et al., 2008; Sturgill et al., 2009; Taft and Turrigiano, 2014) as well as functional (Béïque and Andrade, 2003; Ehrlich and Malinow, 2004; Migaud et al., 1998; Stein et al., 2003) and structural plasticity (Chen et al., 2011; Nikonenko et al., 2008; Steiner et al., 2008). PSD-95 interacts directly with NMDA receptors and through an auxiliary protein stargazin with AMPA receptors (Kornau et al., 1995; Schnell et al., 2002). Interaction of PSD-95 with stargazin regulates the synaptic content of AMPARs (Bats et al., 2007; Chetkovich et al., 2002; Schnell et al., 2002). In agreement with these findings, overexpression of PSD-95 occludes long-term potentiation (LTP) (Ehrlich and Malinow, 2004; Stein et al., 2003) and decreases the threshold for long-term depression (LTD) induction (Béïque and Andrade, 2003). Conversely, mice lacking functional PSD-95 protein have greatly enhanced hippocampal, NMDAR-dependent LTP, whereas NMDAR-dependent LTD is absent (Migaud et al., 1998). Interestingly, the loss-of-function mutant mice lacking the guanylate kinase domain of PSD-95 (Migaud et al., 1998) show normal contextual fear memory but impaired extinction of contextual fear (Fitzgerald et al., 2015), indicating that PSD-95-dependent synaptic plasticity contributes to the updating rather than the formation of contextual fear memory. Here, we hypothesized that PSD-95-dependent synaptic plasticity in dCA1 contributes to the updating aspect of contextual fear memories.

The present study tests this hypothesis by integrated analyses of PSD-95 protein expression and dendritic spines morphology via genetic and chemogenetic manipulations and behavioral studies. We observed that the formation and extinction of contextual fear memory regulate PSD-95 protein expression and dendritic spine remodeling in the dCA1. Using dCA1-targeted overexpression of PSD-95 and chemogenetic manipulations, we show that phosphorylation of PSD-95 at serine 73 is necessary for contextual fear extinction-induced PSD-95 expression and remodeling of dendritic spines. Surprisingly, it is not necessary for fear memory formation or extinction but is required to update partly extinguished fear memories. Overall, our data indicate that the dCA1 PSD-95-driven synaptic processes during the extinction of fear memories enable future updating of the contextual fear memory.

RESULTS

Previous data indicate that loss-of-function mutant mice lacking the guanylate kinase domain of PSD-95 do not show contextual fear extinction, while contextual memory formation is intact (Fitzgerald et al., 2015). Moreover, the contextual fear extinction induces dendritic spine remodeling in the dorsal CA1 area (dCA1) (Garín-Aguilar et al., 2012). Based on these findings, we hypothesise that PSD-95 controls extinction-induced remodeling of dCA1 neuronal circuits supporting contextual fear memory extinction.

Acquisition and extinction of contextual fear memory

To study the synaptic mechanisms of contextual fear extinction memory, we used Pavlovian contextual fear conditioning. Mice were exposed to a new context, and 5 electric shocks (5US) were delivered. The fear memory was extinguished the next day by re-exposure to the same context without the delivery of USs (**Figure** S1). Mice showed low freezing levels in a novel context before delivery of electric shocks (pre-US), and freezing increased during the training (post-US), indicating fear memory formation. Twenty-four hours later, mice were re-exposed for 30 minutes to the training context without the US's presentation for the fear extinction memory session (extinction 1). Freezing levels were high at the beginning of the session, indicating fear memory retrieval and decreased within the session, indicating fear memory extinction formation. Twenty-four hours later, we tested the consolidation fear extinction memory in a second extinction session (extinction 2). At the beginning of extinction 2, freezing levels were lower than at the beginning of extinction 1, indicating long-term fear extinction memory formation. Moreover, the freezing levels further decreased during extinction 2, indicating further updating and extinction of contextual fear memory. Thus, the training-induced robust contextual fear memory was eventually extinguished; however, it required consecutive extinction sessions for attenuation.

The effect of contextual fear extinction memory on PSD-95 expression in dCA1.

To investigate the role of PSD-95 in contextual fear memory consolidation and extinction, we analysed the expression of PSD-95 protein in Thy1-GFP(M) mice (Feng et al., 2000). Thy1-GFP(M) mice express GFP in a sparsely distributed population of the glutamatergic neurons, allowing for dendritic spines visualisation (**Figure** 1A.i). The expression of PSD-95 protein, and its co-localisation with dendritic protrusions, were analysed in three domains of dCA1: stratum oriens (stOri), stratum radiatum (stRad) and stratum lacunosum-moleculare (stLM) (**Figure** 1A.ii-iii). We analysed these regions separately as previous data found dendrite-specific long-term dendritic spines changes after contextual fear conditioning (Restivo et al., 2009).

Thy1-GFP(M) mice underwent contextual fear conditioning. They showed low freezing levels in the novel context before delivery of electric shocks, after which freezing levels increased the remainder of the training session (**Figure** 1B) (RM ANOVA, effect of time: $F(1, 7) = 734.1$, $P < 0.0001$). Twenty-four hours later, one group of mice was sacrificed (5US), and the second group was re-exposed to the training context without presentation of US for extinction (Ext). Freezing levels were high at the beginning of the session and decreased within the session, indicating the formation of fear extinction memory (**Figure** 1B) ($t = 3.720$, $df = 6$, $P < 0.001$). Mice were sacrificed immediately after the fear extinction session (Ext). As controls, naïve mice were taken from their home cages. The analysis of PSD-95 immunostaining revealed a significant effect of training (RM ANOVA, $F(2, 22) = 7.69$, $P = 0.003$) and dCA1 region ($F(1.317, 18.44) = 141.0$; $P < 0.001$) on PSD-95 expression per dendritic spine (**Figure** 1C.i,ii). *Post hoc* tests indicated that in the stOri and stLM, PSD-

95 expression decreased in the 5US group, compared to the Naïve mice (Tukey's multiple comparisons test, stOri: $P = 0.004$; stLM: $P = 0.038$), and increased after extinction (Ext), compared to 5US group (stOri: $P = 0.019$; stLM: $P = 0.009$) (**Figure** 1C.ii). No difference in PSD-95 levels was observed in stRad between the groups. Thus, our data show that both the formation and extinction of contextual fear memory regulate PSD-95 levels in dCA1 strata, and the effect is specific to stOri and stLM regions.

Since PSD-95 is expressed in large and mature spines (El-Husseini et al., 2000), we checked whether the changes in PSD-95 levels were associated with dendritic spine remodeling. We did not observe a significant effect of training (RM ANOVA, $F(2, 48) = 3.149$, $P = 0.052$), but we did discover a region effect ($F(1.788, 42.92) = 7.381$, $P = 0.002$) and training × region interaction ($F(4, 48) = 5.48$, $P = 0.001$) on dendritic spines density (**Figure** 1D). In stOri, dendritic spines density decreased after fear extinction training (Ext) compared to the trained mice (5US) (Tukey's test, $P = 0.025$) (**Figure** 1D.i-iii). In stLM, dendritic spine density was increased in the Ext group compared to the Naïve mice ($P = 0.039$). No changes in spine density were observed in the stRad. Moreover, we observed a significant effect of training on the median area of dendritic spines in the stOri (Kruskal-Wallis test, $H = 8.921$, $P = 0.012$) and stLM ($H = 28.074$, $P < 0.001$), but not stRad ($H = 5.919$, $P = 0.744$) (**Figure** 1D.iv). In stOri, the median spine area was decreased in the 5US group compared to the Naïve mice (Dunn's multiple comparisons test, $P = 0.032$) and increased after extinction (Ext) compared to the 5US group ($P = 0.02$). In stLM, the median spine area did not change after training (5US), compared to the Naïve mice ($P > 0.05$), but increased after extinction (Ext), compared to the 5US group ($P = 0.005$). Thus, increased expression of PSD-95 in stOri and stLM during contextual fear extinction was coupled with an increased median spine area. Overall, our data indicate a remodeling of the dCA1 neuronal circuits during contextual fear extinction that presumably involves extinction-induced upregulation of PSD-95 expression.

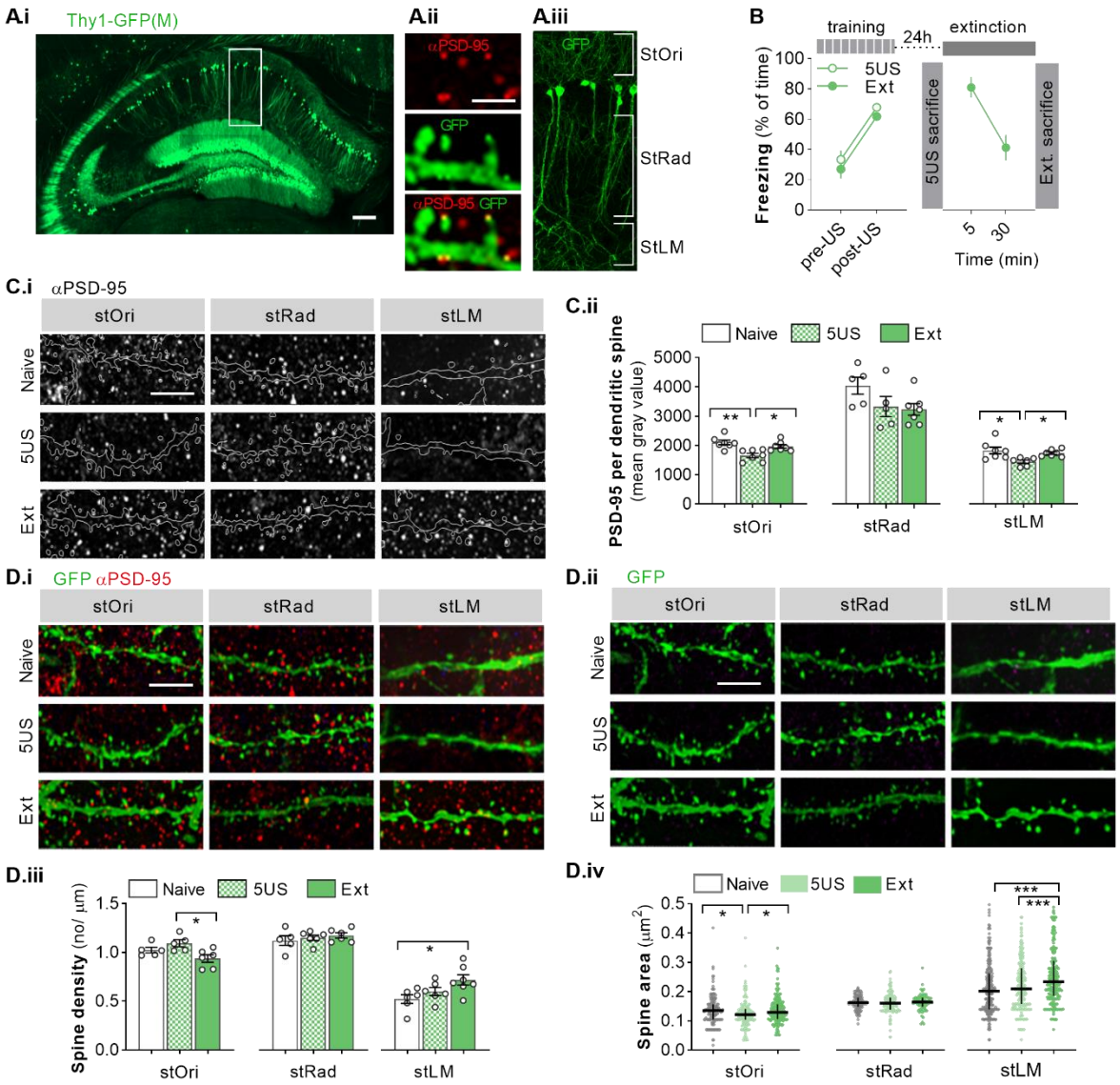

Figure 1. Formation and extinction of contextual fear memory regulate expression of synaptic PSD-95 protein and remodeling of dendritic spines in dCA1. (A) Dendritic spines were analysed in three domains of dendritic tree of dCA1 area in Thy1-GFP(M) mice: stOri, stRad and stLM. **(i)** Microphotography of dCA1 of a Thy1-GFP(M) mouse. **(ii)** High magnification of confocal scans showing colocalization of PSD-95 immunostaining and dendritic spines. **(iii)** Division of dCA1 dendritic tree domains. **(B)** Experimental timeline and freezing levels of mice from two experimental groups: fear conditioning training (5US) only and fear extinction (Ext). **(C) (i)** Representative confocal images of PSD-95 immunostaining (maximum projections of z-stacks composed of 20 scans) are shown for three domains of the dendritic tree. (**ii**) Summary of data showing PSD-95 expression in stOri (mouse/spine: Naïve = 6/579; 5US = 6/807; Ext = 7/986), stRad (mouse/spine: Naïve = 6/571; 5US = 6/619; Ext = 7/712), and stLM (mouse/spine: Naïve = 6/705; 5US = 6/650; Ext = 7/925). **(D) (i-ii)** Representative confocal images of dendrites colocalized with PSD-95 immunostaining from Thy1-GFP(M) mice that underwent training are shown for three domains of the dendritic tree. **(iii)** Summary of data showing dendritic spines density in stOri (mouse/dendrite: Naïve = 6/16; 5US = 6/24; Ext = 7/34), stRad (mouse/dendrite: Naïve = 6/18; 5US = 6/20; Ext = 7/19), and stLM (mice/dendrite: Naïve = 6/31; 5US = 6/25; Ext = 7/37). **(iv)** Summary of data showing average dendritic spine area in stOri, (mice/ spines: Naïve = 6/579; 5US = 6/807; Ext = 7/986), stRad (mouse/spine: Naïve = 6/571; 5US = 6/619; Ext = 7/712), and stLM (mouse/spine Naïve = 6/705; 5US = 6/650; Ext = 7/925). For C.ii and D.iii, each dot represents one mouse. For D.iv, each dot represents one dendritic spine. Scale bars: A.i: 0.5 mm, A.ii: 8 µm, C and D: 15 µm. *P < 0.05, **P < 0.01; ***P < 0.001.

The role of dCA1 PSD-95(S73) phosphorylation in regulation of memory extinction-induced PSD-95 expression.

Based on the observed changes of PSD-95 levels and dendritic spines in dCA1 during contextual fear extinction, we hypothesized that extinction-induced upregulation of PSD-95 enables remodeling of the necessary circuits for contextual fear extinction memory. To validate this hypothesis, we used dCA1-targeted overexpression of phosphorylation-deficient PSD-95, with serine 73 mutated to alanine [PSD-95(S73A)]. We focused on serine 73 as its phosphorylation by CaMKII negatively regulates activity-induced spine growth (Gardoni et al., 2006; Steiner et al., 2008) and αCaMKII autophosphorylation-deficient mice have impaired contextual fear memory extinction and updating (Radwanska et al., 2011). Accordingly, we expected that overexpression of PSD-95(S73A) would escalate fear extinction-induced accumulation of PSD-95 and spine growth. We did not use a phospho-mimetic form of PSD-95 (S73D), as this mutant protein locates mostly in dendrites in our hands (data not shown) and, therefore, unlikely affects synaptic function.

We designed and produced adeno-associated viral vectors, isotype 1 and 2 (AAV1/2) encoding mCherry under αCaMKII promoter (Control), wild-type PSD-95 protein fused with mCherry (AVV1/2:CaMKII_PSD-95(WT):mCherry) (WT) and phosphorylation-deficient PSD-95, where serine 73 was changed for alanine, fused with mCherry, (AVV1/2:CaMKII_PSD-95(S73A):mCherry) (S73A). We did not use a PSD-95 shRNA and shRNA-resistant PSD-95 genetic replacement strategy (Steiner et al., 2008) as these viruses depleted total PSD-95 levels *in vivo* in our hands (data not shown). The Control, WT and S73A viruses were stereotactically injected into the dCA1 of C57BL/6J mice (**Figure** 2A). Viral expression was limited to the dCA1 (**Figure** 2B). Expression of WT and S73A viruses resulted in significant overexpression of PSD-95 protein in three domains of a dendritic tree, compared to the Control virus (**Figure** 2C) (effect of virus: $F(2, 30) = 13.09$, $P < 0.0001$). Correlative light and electron microscopy confirmed that the overexpressed PSD-95 (WT and S73A) co-localised with postsynaptic densities (PSDs) of postsynaptic glutamatergic synapses (**Figure** 2D). Therefore, we next investigated how fear extinction memory affects exogenous PSD-95 protein expression.

A new cohort of mice with dCA1-targeted expression of the Control, WT and S73A groups underwent contextual fear conditioning (**Figure** 2E). Mice in all experimental groups showed increased freezing levels at the end of the training (RM ANOVA, effect of training: $F(1, 30) = 269.4$, $P < 0.001$, effect of virus: $F(2, 30) = 2.815$, $P = 0.076$) (**Figure** 2E.i). Half of the mice were sacrificed 24 hours after the fear conditioning (5US). The remaining half were re-exposed to the training box for fear extinction and sacrificed immediately afterward (Ext). All animals showed high freezing levels at the beginning of the session, which decreased during the session indicating the formation of fear extinction memory (RM ANOVA, effect of training: $F(1, 15) = 65.68$, $P < 0.001$). Surprisingly, no effect of the virus was found ($F(2, 15) = 0.993$, $P = 0.393$) (**Figure** 2E.ii).

For each animal, half of the brain was chosen at random for confocal analysis of the overexpressed PSD-95 protein, and the other half was processed for serial face-block scanning electron microscopy (SBEM) to analyse synapses at nanoscale resolution (Denk and Horstmann, 2004; Hughes et al., 2014) (**Figure** 2F). The AAVs penetrance did not differ between the experimental groups (5US vs Ext) and reached over 80% in the analysed sections of dCA1 (**Figure** 2G). To assess the effect of the fear extinction memory session on the exogenous PSD-95 (WT and S73A) protein levels, we analysed fluorescent, synaptic-like puncta formed by mCherry fused with PSD-95 protein (**Figure** 2H.i (inset)). Three-way ANOVA indicated a significant effect of the training ($F(1, 52) = 11.36$, $P = 0.0014$) and dCA1

domain ($F(2, 52) = 8.677$, $P = 0.006$) on the expression of PSD-95:mCherry, but no effect of the virus ($F(1, 52) = 0.8200$, $P = 0.369$). *Post hoc* LSD analysis for the planned comparisons revealed that WT expression was upregulated in stOri and stLM, but not stRad, after the extinction session (Ext), compared to the 5US group ($P < 0.001$) (**Figure** 2H.iii). Thus, the exogenous PSD-95(WT) protein levels were upregulated during fear extinction training in the same way as endogenous PSD-95. Surprisingly, no significant difference in the exogenous PSD-95(S73A) levels was observed between the Ext and 5US groups in all three strata of dCA1 (**Figure** 2H.iii). Therefore, our data indicate that phosphorylation of PSD-95 at S73 is necessary for the fear extinction-induced upregulation of PSD-95 levels, although it does not affect the formation, consolidation and extinction of contextual fear memory.

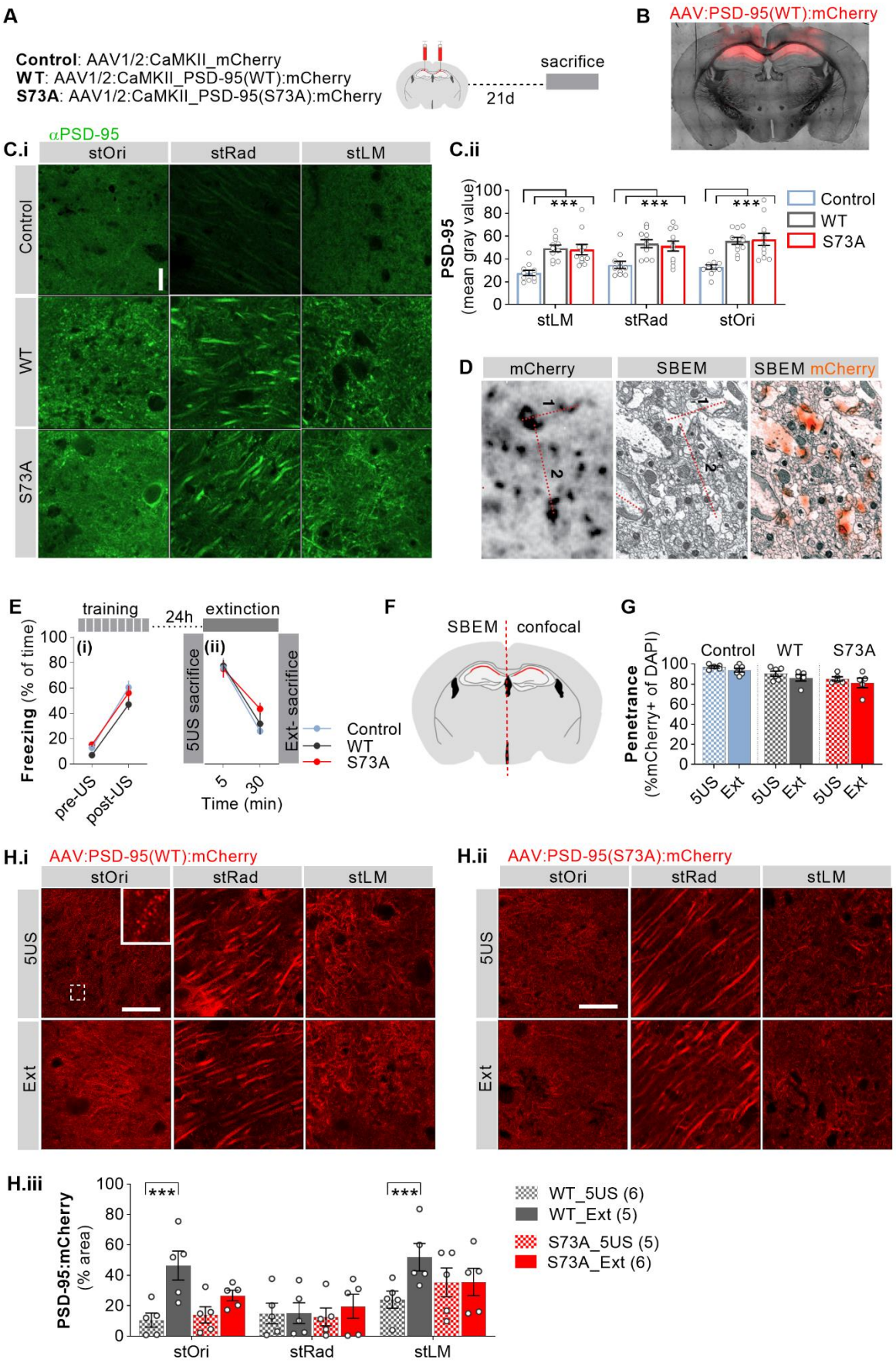

Figure 2. Phosphorylation of PSD-95(S73) is required for upregulation of PSD-95 levels during fear extinction training. (A) Mice were stereotactically injected in the dCA1 with AAV1/2 encoding

Control (mCherry), PSD-95(WT) (WT) or PSD-95(S73A) (S73A). **(B)** Microphotography of a brain with dCA1 PSD-95(WT):mCherry (WT) expression. **(C)** Analysis of PSD-95 overexpression. **(i)** Representative confocal scans of the brain slices immunostained for PSD-95. Scale bar, 10 µm. **(ii)** Quantification of local expression of PSD-95 in three domains of dCA1 in mice with Control, WT and S73A. **(D)** Overexpressed WT co-localises with postsynaptic densities. Single confocal scan of overexpressed WT in dCA1 (left), SBEM scan of the same area (middle) and superposition of confocal (orange) and SBEM images based on measured distances between large synapses (1 & 2) (right). Measurements: (confocal image) 1: 3.12 µm, 2: 4.97 µm; (SBEM image) 1: 2.98 µm, 2: 4.97 µm. **(E)** Experimental timeline and percentage of freezing during **(i)** fear conditioning (5US) and **(ii)** fear extinction (Ext) session of mice with dCA1-targeted expression of Control, WT or S73A. **(F)** Illustration of the brain processing scheme **(G)** Summary of data showing penetrance of the viruses in dCA1 (sections used for confocal and SBEM analysis). **(H)** Expression of the exogenous PSD-95 in dCA1. **(i-ii)** Representative, confocal scans of the fused mCherry protein in three strata of dCA1. Inset: magnification of a dashed line rectangle. Scale bars, 10 µm. (**iii**) Quantification of the PSD-95:mCherry-positive puncta. For C.ii, G and H.iii, each dot on the graphs represent one mouse. ***P < 0.001.

The role of PSD-95(S73) phosphorylation in regulating extinction-induced synapse remodeling.

Since phosphorylation of PSD-95 at S73 is required for the fear extinction-induced upregulation of PSD-95, we hypothesized that PSD-95 also regulates extinction-induced synaptic growth. To test this, we used SBEM to determine dendritic spines density and to reconstruct spines and PSDs in the stOri (**Figure** 3A.i-iii). PSDs are the postsynaptic elements that scale up with synaptic strength and are visible in electron microphotographs. In total, we reconstructed 159 spines from the brains of the mice expressing WT sacrificed 24 hours after contextual fear conditioning (5US) (n=3), and 178 spines from the mice sacrificed after fear extinction (Ext) (n=3). For mice expressing S73A, 183 spines were reconstructed in the 5US group (n=3) and 160 Ext (n=3). Lastly, we reconstructed 364 dendritic spines and PSDs in the Control 5US mice (n=3), and 293 spines from Ext (n =3). Figure 3B shows reconstructions of dendritic spines from representative SBEM brick scans for each experimental group.

Overexpression of PSD-95 protein (WT and S73A) resulted in decreased dendritic spines density and increased surface area of PSDs, compared to the Control group (**Figure** S2). We also observed a significant effect of the training on dendritic spines density ($F(1, 45) = 8.01$, $P = 0.007$). *Post hoc* analysis showed that the dendritic spines density was downregulated in the Control and WT Ext groups compared to their respective 5US groups (Fisher's LSD test for planned comparisons, $P < 0.035$ and $P < 0.014$). No significant difference was observed for S73A Ext and 5US groups (**Figure** 3C). Furthermore, the median value of PSD surface areas was increased after the extinction training in the Control and WT groups (Mann-Whitney test, $U = 42410$, $P < 0.001$ and $U = 9948$, $P < 0.001$), but not in the S73A group ($U = 13578$, $P = 0.246$) (**Figure** 3D). The changes of PSDs surface area after extinction compared to 5US groups were also indicated as shifts in the frequency distribution toward bigger values in Control and WT groups **(Figure** 3E.i-ii**)**, but not in S73A (**Figure** 3E.iii). Lastly the upward shift of the correlation lines of spine volume and PSD surface area after extinction training in Controls (ANCOVA, elevation: $F(1, 6) = 4.677$, $P = 0.031$) and WT groups (elevation: $F(1, 319) = 4.256$, $P = 0.039$), compared to their respective 5US groups (**Figure** 3F.i-ii). Therefore, dendritic spines had relatively bigger PSDs after fear extinction than the dendritic spines of the same size in the 5US groups. Such shift was not observed in the mice overexpressing S73A (elevation: $F(1, 340) = 0.603$, $P = 0.437$) (**Figure** 3F.iii). Thus, in Control and WT groups, as in Thy1-GFP mice, elimination of dendritic

spines observed after fear extinction was accompanied by an increased median area of the remaining synapses, indicating remodeling of the dCA1 circuits. The overexpression of S73A impaired both fear extinction-induced synaptic elimination and synaptic growth. We also confirmed the effect of PSD-95-overexpression and fear extinction training on synaptic transmission in dCA1 using *ex vivo* field recordings. We observed that after fear extinction the amplitude of field excitatory postsynaptic potentials (fEPSPs) was increased in the stOri dCA1 (when Shaffer collaterals were stimulated) of the mice that overexpressed PSD-95(WT), compared to their respective 5US groups (**Figure** S3), indicating enhanced excitatory synaptic transmission. Such change was not seen in S73A mice. There was also no effect of the extinction training on the fiber volley in both WT and S73A groups. Altogether, the electrophysiological analysis shows that PSD morphologic changes and functional alterations of synapses confirm the role of PSD-95 in remodeling of dCA1 circuits in contextual fear extinction (**Figure** S3E.i,ii).

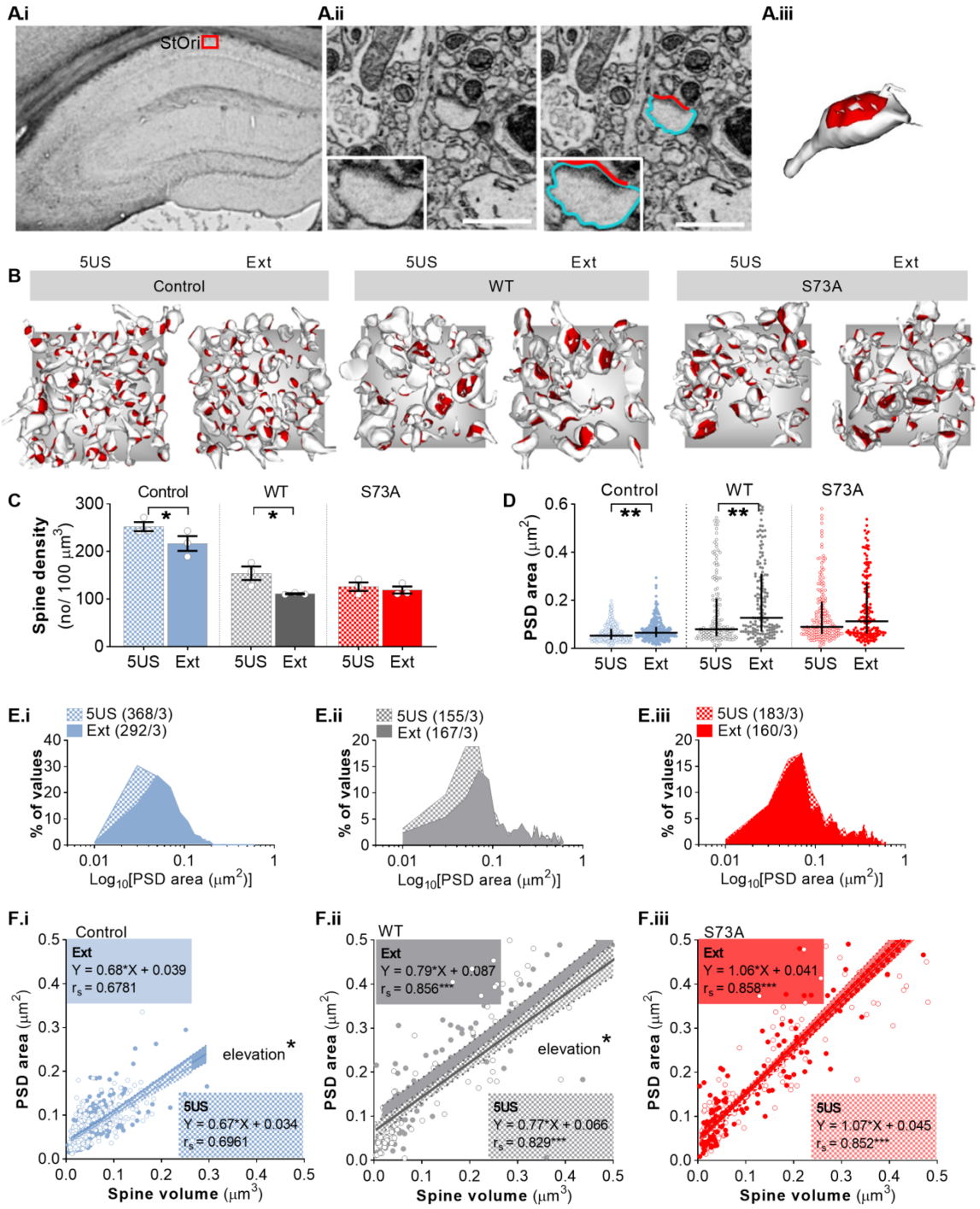

Figure 3. Phosphorylation of PSD-95 at S73 is required for synapse elimination and growth of remaining PSDs in stOri after fear extinction training. (**A**) The principles for SBEM analysis of the ultrastructure of dendritic spines and PSDs. **(i)** Microphotography of a dorsal hippocampus with the region of interest for analysis; **(ii)** Tracing of a dendritic spine and PSD. Scale bars, 0.5 µm. A representative traced dendritic spine (in blue) and its PSD (in red), and **(iii)** the reconstruction of this spine. **(B)** Exemplary reconstructions of dendritic spines and their PSDs from SBEM scans. The grey background rectangles are x = 4.3 × y = 4.184 µm. Dendritic spines and PSDs were reconstructed and analysed in tissue bricks **(C)** Mean density of dendritic spines was downregulated after fear extinction (Ext) compared to (5US) trained Control and PSD-95(WT) (WT) but not PSD-95(S73A) (S73A) groups. **(D)** Median PSD surface area was increased after fear extinction (Ext) in Control and WT mice but did not change in S73A group (**E**) Distributions were shifted towards bigger values in **(i)** Control and **(ii)** WT groups **(iii)** but not in the S73A group. X axes are Log_{10}-transformed to show the

differences between the groups. **(F)** Graphs showing changes in the correlation of dendritic spine volume and PSD surface area in **(i)** Control **(ii)** WT **(iii)** and S73A groups before (5US) and after extinction (Ext) training. For D, each dot represents an individual dendritic spine; medians with IQR are shown. ***P < 0.001, **P < 0.01, *P < 0.05.

The role of dCA1 PSD-95(S73) phosphorylation in contextual fear extinction memory.

Since overexpression of phosphorylation-deficient PSD-95(S73A) impaired extinction-induced expression of PSD-95 and structural and functional changes of synapses but did not affect fear extinction memory, we hypothesised that PSD-95-dependent remodeling of synapses is necessary for consolidation of fear extinction memory. To test this hypothesis, a new cohort of mice with dCA1-targeted expression of the Control virus, WT or S73A, underwent fear conditioning and fear extinction training. The post-training analysis showed that the viruses were expressed in dCA1 (**Figure** 4A.i). The Control virus was expressed in 98% of the dCA1 cells, WT in 88% and S73A in 83% (effect of virus: $F(2, 30) = 10.82$, $P = 0.0003$) (**Figure** 4A.ii-iii). Overexpression of PSD-95 (WT and S73A) did not affect mice basal activity or freezing during training (RM ANOVA, effect of virus: $F(2, 25) = 1.224$, $P = 0.311$) (**Figure** 4B.i). In all experimental groups freezing levels increased during training (effect of time: $F(1, 25) = 181.5$, $P < 0.001$; genotype: $F(2, 57) = 2.899$, $P = 0.063$) (**Figure** 4B.i). When mice were placed in the same context 24 hours later, their initial freezing levels were high and did not differ between the groups, indicating a similar level of fear memory acquisition (**Figure** 4B.ii). Throughout the test, mice from all groups exhibited a within-session decrease of freezing levels that is typical of extinction memory formation (effect of training: $F(1, 22) = 55.32$, $P < 0.001$) (**Figure** 4B.ii). As in the previous experiment, there was no virus effect ($F(2, 42) = 1.994$, $P = 0.149$). Thus, neither overexpression of the WT or S73A forms of PSD-95 affected the formation or extinction of contextual fear memory.

To assess the persistence of the consolidated fear extinction memory, mice were re-exposed to the training context 24 hours later. There was no difference in the freezing levels between the groups at the beginning of the extinction session, indicating no impairment of consolidation and retrieval of fear extinction memory (**Figure** 4B.iii). However, there was a significant effect of time ($F(1, 22) = 8.756$, $P = 0.007$) and interaction of the virus and time on the freezing levels ($F(2, 22) = 5.128$, $P = 0.015$). As confirmed by Tukey's multiple comparisons test, at the end of the session S73A mice showed higher freezing levels than the Control ($P = 0.020$) and WT ($P = 0.024$) groups (**Figure** 4B.iii). Thus, our data indicate that overexpression of S73A in dCA1 does not affect fear memory formation, recall, or extinction but prevents the updating of a partly extinguished contextual fear memory.

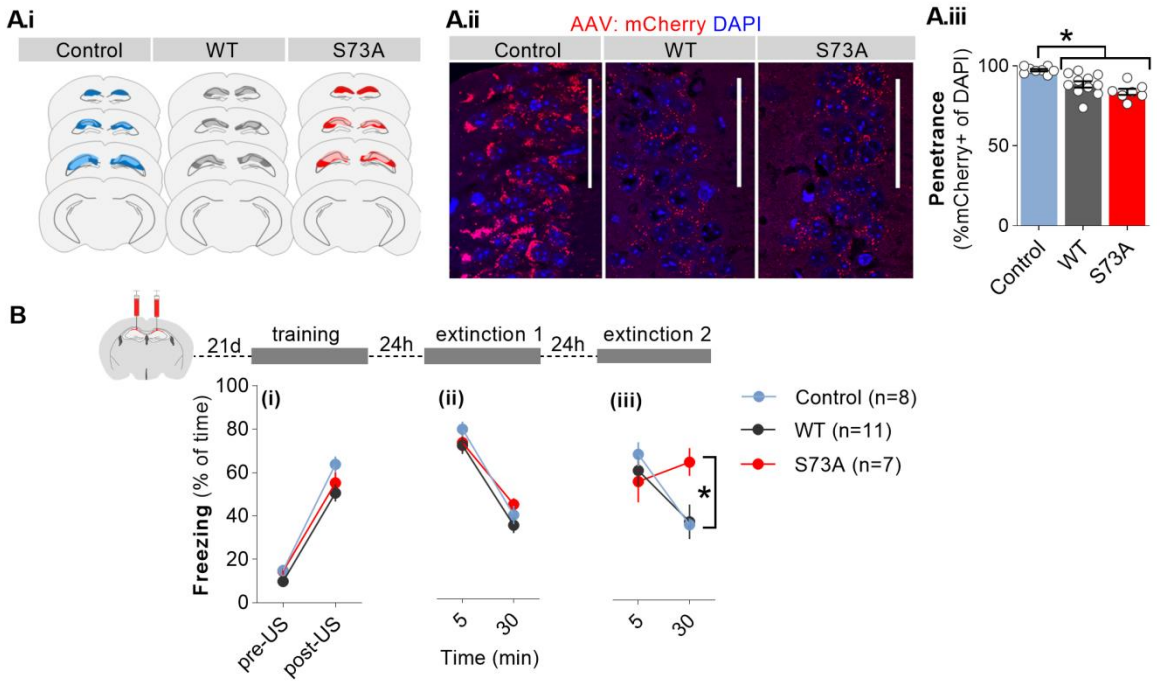

Figure 4. Phosphorylation of PSD-95 at serine 73 is required to update a partly extinguished fear memory. A (i) Area and extent of viral infection shown. **(ii)** Single confocal scans of the stratum pyramidale of dCA1 of the mice expressing Control (mCherry), PSD-95 (WT) and (S73A) (scale bars, 50 µm) and **(iii)** penetrance of the viruses. **(B)** Experimental timeline and percentage of freezing during fear conditioning **(i)** and fear extinction sessions **(ii and iii)** of the mice with dCA1-targeted expression of Control, WT or S73A. *P < 0.05.

Effect of chemogenetic inhibition of dCA1 on fear extinction-induced expression of PSD-95.

Our data indicate that PSD-95(S73A) overexpression prevents extinction-induced upregulation of PSD-95 and synaptic remodeling, as well as the updating of a partly extinguished fear memory. These observations suggest that extinction-induced upregulation of PSD-95 is required to update an extinguished fear memory. However, behavioral impairments induced by overexpression of S73A may result from the deregulation of PSD-95 levels at other time points of training. Accordingly, we asked whether the dCA1 activity, specifically during the first extinction session, is required for extinction-induced PSD-95 expression. Such findings would support the hypothesis that extinction-induced PSD-95 expression is required to update a partly extinguished fear memory.

To test this hypothesis we used chemogenetic tools to manipulate dCA1 activation during the fear extinction memory session and analysed extinction-induced PSD-95 expression. AAV1/2 encoding inhibitory designer receptors exclusively activated by designer drugs (DREADD, hM4(Gi)) under human synapsin (hSyn) promoter [AAV1:hSyn-hM4(Gi):mCherry (hM4)] (Lee et al., 2014), or a Control virus encoding mCherry (AAV1/2:CaMKII-mCherry) were bilaterally infused into the dCA1 region of mice. The post-training analysis of the hippocampal sections confirmed that the expression of the viruses was limited to the dCA1 (Bregma > -2.5 mm) (**Figure** 5A). There were no significant differences in the virus penetration between the experimental groups [hM4 was expressed in 71% and 80% of the pyramidal cells (in the saline and CNO groups, respectively); the Control virus

was expressed in 84% and 87% of the cells (saline and CNO, respectively)] (**Figure** 5B). Both groups of the mice with hM4 virus showed low freezing levels at the beginning of the training session, and freezing increased after USs delivery (RM ANOVA, effect of time: $F(1, 10) = 86.36$, $P < 0.0001$) (**Figure** 5C.i). The next day, mice received a systemic injection of saline or CNO, and 30 minutes later, they were re-exposed to the training context. As in previous experiments, both groups of mice showed high levels of feezing at the beginning of the extinction session, which decreased throughout the session (effect of time: $F(1, 11) = 8.149$, $P = 0.016$), indicating the formation of fear extinction memory. There was no effect of drug ($F(3, 26) = 2.438$, $P = 0.087$), or a training and drug interaction ($F(3, 26) = 1.086$; $P = 0.372$), on the freezing levels (**Figure** 5C.i). At the end of the 30-minute extinction session, the brains were collected and immunostained to detect PSD-95 protein (**Figure** 5C.ii). There was a significant effect of drug ($F(1, 16) = 31.06$, $P < 0.0001$), but no effect of the CA1 domain ($F(2, 29) = 0.739$, $P = 0.486$), on PSD-95 levels. *Post hoc* Sidak's tests confirmed that the expression of PSD-95 was decreased in all dCA1 domains in the CNO group, compared to the saline-treated animals ($P < 0.05$ for all domains) (**Figure** 5C.iii). To validate whether this downregulation of PSD-95 expression was specific to the chemogenetic inhibition, we trained mice with the Control virus expressed in the dCA1 (**Figure** 5D). The animals were injected with CNO before the extinction session and sacrificed after the session (**Figure** 5D.i). As in the previous experiment, CNO did not affect memory recall or fear extinction (effect of drug: $F(3, 27) = 1.628$, $P = 0.206$). Moreover, there was no significant effect of the drug (RM ANOVA, effect of drug: $F(1, 12) = 3.73$, $P = 0.077$) or the region ($F(1.302, 14.32) = 1.505$, $P = 0.248$) on PSD-95 expression levels (**Figure** 5D.ii-iii), indicating that CNO does not affect PSD-95 expression.

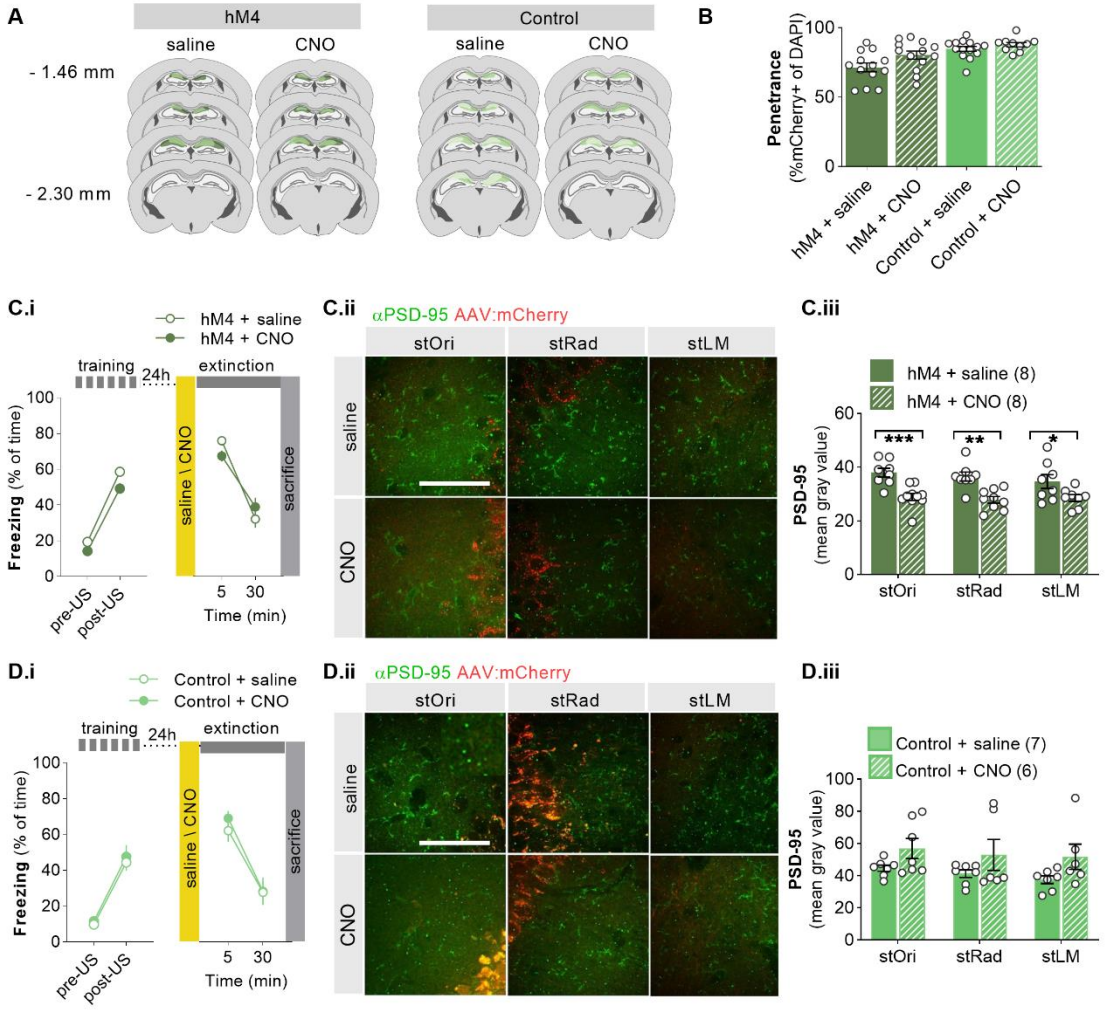

Figure 5. Chemogenetic inhibition of dCA1 during extinction session impairs extinction-induced PSD-95 expression. Three weeks after bilateral dCA1 viral infusion surgery, mice were trained in fear conditioning, followed by a fear extinction session 24 hours later. In all groups, saline or CNO was systemically injected 30 minutes before the extinction session. Mice were sacrificed immediately after the fear extinction session. **(A)** The extent of viral transfections in the CA1 area. **(B)** Penetrance of hM4 virus and Control virus in dCA1. **(C) (i)** Experimental timeline and percentage of freezing during fear conditioning and fear extinction session of the mice with hM4 virus. **(ii)** Representative, confocal scans of the brain slices immunostained for PSD-95. Scale bar: 10 µm. **(iii)** Summary of data quantifying the expression of PSD-95 in three domains of dCA1 of the mice with hM4 virus. **(D) (i)** Experimental timeline and percentage of freezing during fear conditioning and fear extinction session of the mice with the Control virus. **(ii)** Representative, confocal scans of the brain slices immunostained for PSD-95. Scale bar: 10 µm. **(iii)** Summary of data quantifying the expression of PSD-95 in three domains of dCA1 of the mice with the Control virus. *P < 0.05, **P < 0.01; ***P < 0.001.

Since dendritic spines in dCA1 undergo constant remodeling (Attardo et al., 2015) the effect of the chemogenetic inhibition of dCA1 neurons on PSD-95 levels could be unrelated to the extinction-induced PSD-95 expression but results from decreased cell activity. To test this hypothesis we chemogeneticaly inhibited dCA1 neurons outside of the fear extinction time-window (7d after extinction 2) and measured the changes of PSD-95. Mice with bilateral expression of hM4 or the Control virus were systemically injected with saline or CNO

(**Figure** S4). As in the extinction experiment, the brains were collected 60 minutes after the injection and immunostained for PSD-95. At this time point, no effect of the drug on PSD-95 levels was observed in the Control or hM4 groups (**Figure** S4). Thus, chemogenetic inhibition of dCA1 outside of the fear extinction memory window does not affect the levels of PSD-95.

The effect of chemogenetic inhibition of dCA1 area during fear extinction on updating an extinguished contextual fear memory.

Overall, our experiments showed that chemogenetic inhibition of dCA1 during extinction of contextual fear memory prevented the extinction-induced expression of PSD-95. Thus extinction-induced upregulation of PSD-95 levels in the dCA1 is a likely mechanism that enables future updating of the consolidated contextual fear memory. To test this hypothesis, we again used chemogenetic tools. Mice were bilaterally injected in the dCA1 with AAV1/2 encoding hM4 or the Control virus, and they were trained 3 weeks later (**Figure** 6A.i). The post-training analysis of the hippocampal sections revealed that hM4 was expressed in 76% of the pyramidal cells of dCA1 (both in cell bodies and dendrites), while the Control virus in 84% of the cells (**Figure** 6A.ii-iii). The expression of the virus was limited to the dCA1 (Bregma > -2.5 mm) (**Figure** 6B). Three weeks post-surgery and viral infection, mice underwent contextual fear conditioning, followed by fear extinction (**Figure** 6C-D).

During fear conditioning training, mice exhibited low freezing levels before the first conditioning trial (pre-US), and freezing levels increased across the conditioning session in all experimental groups (RM ANOVA, effect of training, hM4: $F(1, 10) = 86.36$, $P < 0.0001$; Control: $F(1, 12) = 68.13$, $P < 0.0001$) (**Figure** 6C-D.i). Freezing levels did not differ between the drug groups indicating similar levels of conditioned fear (effect of drug: hM4: $F(1, 10) = 0.604$, $P = 0.454$; Control: $F(1, 12) = 0.836$, $P = 0.378$). Twenty-four hours after training, mice received a systemic injection of saline or CNO (1 mg/kg) to activate hM4 receptors, and were re-exposed to the training context. Mice in all groups showed initial high freezing levels, indicating fear memory formation and no drug-induced impairment of memory recall ($P > 0.05$ for hM4 and Control) (**Figure** 6C-D.ii). Freezing levels in all groups decreased throughout the session indicating fear memory extinction (effect of time: hM4: $F(1, 9) = 9.87$, $P = 0.011$; Control: $F(1, 12) = 66.76$, $P < 0.0001$). There was no effect of the drug on the freezing levels in any of the virus groups (hM4: $F(1, 9) = 0.168$, $P = 0.691$; Control: $F(1, 12) = 1.279$, $P = 0.280$) (**Figure** 6C-D.ii), indicating that neither CNO nor chemogenetic inhibition of dCA1 affect fear extinction.

We next tested long-term fear extinction memory retrieval 24 hours later in a second extinction session (extinction 2). In hM4 groups, the freezing levels were low at the beginning of extinction 2, indicating that chemogenetic inhibition of dCA1 did not impair fear extinction memory consolidation (**Figure** 6C.iii). However, freezing levels decreased throughout the session only in the saline group, but not in the mice injected with CNO the previous day. This observation was confirmed by a significant interaction between time and drug ($F(1, 9) = 6.252$, $P = 0.033$) and *post hoc* Sidak's multiple comparisons tests, which found a significant difference between the drug groups at the end of the session ($P = 0.014$) (**Figure** 6C.iii). In the Control virus groups, the initial low freezing levels further decreased during the session, and no effect of the drug was observed (effect of time: $F(1, 15) = 5.92$, $P = 0.027$; effect of drug: $F(1, 15) = 0.032$, $P = 0.860$) (**Figure** 6D.iii). Thus, CNO alone did not affect consolidation or updating of fear extinction memory. However, chemogenetic inhibition of dCA1 impaired contextual fear memory updating during the second extinction session.

Therefore, we next asked whether chemogenetic manipulation of dCA1 outside (a day prior) the fear extinction memory session (extinction 1) impairs updating of the fear memory.

A new group of C57BL/6J mice were injected into dCA1 with AAV1/2 encoding hM4 or Control virus and trained 3 weeks later (**Figure** 6E). The virus penetrance and area of the infection were similar to previous experiments. Both groups of mice demonstrated higher freezing levels at the end of training indicating fear memory formation (effect of training: $F(1, 14) = 270$, $P < 0.0001$; virus: $F(1, 14) = 0.962$, $P = 0.343$) (**Figure** 6E.i). The next day, all mice received a systemic injection of CNO and were re-exposed to the training context 24 hours later. In extincion 1, mice from both groups showed initial high freezing levels, which decreased throughout the session (effect of training: $F(1, 14) = 270$, $P < 0.0001$). No significant effect of the virus on the freezing levels was observed ($F(1, 15) = 0.134$, $P = 0.719$), indicating no impairment of fear memory recall and extinction (**Figure** 6E.ii). In the second extinction session, initial freezing levels were low, further decreasing during the session (effect of training: $F(1, 14) = 6.832$, $P = 0.02$). Again no significant effect of the virus was observed ($F(1, 14) = 0.306$, $P = 0.588$), indicating that inhibition of dCA1 outside of the extinction session did not affect the future updating of fear memory (**Figure** 6E.iii). Overall, our data indicate that chemogenetic inhibition of dCA1 during the contextual fear extinction session does not affect fear memory recall or extinction but prevents future updating of the contextual fear memory leading to fear memory persistence.

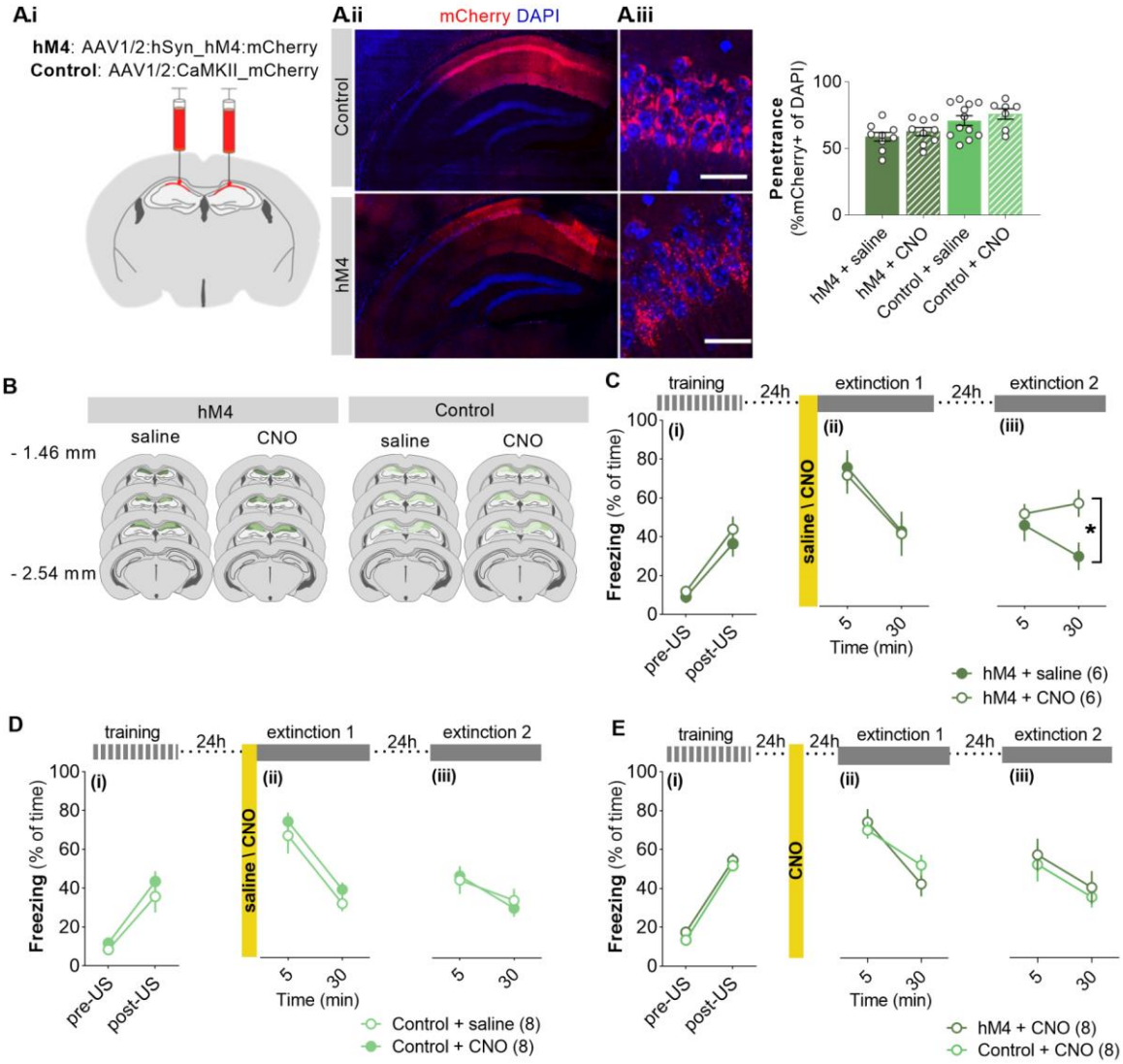

Figure 6. Chemogenetic inhibition of dCA1 impairs updating of partly extinguished fear memory. (A) (i) AAV-hSyn-hM4(Gi):mCherry (hM4) and Control virus (mCherry) were bilaterally injected into the dCA1 (left). **(ii)** Single confocal scans showing transfected dCA1. Viral expression was observed in cell bodies and dendrites of pyramidal neurons. **(iii)** Magnification of dCA1 confocal scans (Scale bars, 30 μm) and penetrance of hM4 virus (n = 27 animals) and Control virus (n = 24 animals). **(B)** The extent of viral transfections in the CA1 area. Minimum and maximum transfections are shown. **(C-D)** Experimental design and percentage of freezing during fear conditioning and fear extinction sessions (1 and 2) of the mice with hM4 **(C)** and Control virus **(D)**. Mice were trained three weeks after the surgery for optimal virus expression. In all groups, saline or CNO was systemically injected 30 minutes before extinction 1. **(E)** Experimental design and percentage of freezing during fear conditioning and fear extinction sessions (1 and 2) of the mice with Control or hM4 virus. Mice were trained three weeks after the surgery and virus expression. In all groups CNO was systemically injected 24 hours before extinction 1 in all groups. *P < 0.05, LSD test for planned comparisons only, CNO vs. saline. For C-E, numbers of trained mice are indicated in the legends.

DISCUSSION

Here, we have investigated synaptic processes in the dCA1 that contribute to contextual fear memory attenuation. Our interest in this problem stems from many anxiety

disorders associated with impaired fear extinction and hippocampus function (van Rooij et al., 2018). The key findings from the present study are that (1) contextual fear extinction memory increases PSD-95 protein expression in the dCA1 that is accompanied by remodeling of the glutamatergic synapses; (2) this extinction-induced PSD-95 expression and synaptic remodeling are regulated by phosphorylation of PSD-95 at serine 73; (3) both PSD-95 phosphorylation at serine 73 and cellular activity in the dCA1 during contextual fear extinction is required for the updating of partly extinguished fear memories but not for the initial attenuation of the fear memory. Below, the significance of the findings is discussed in light of previous studies.

The formation of spatial and contextual fear memories is thought to involve NMDA receptor-dependent synaptic plasticity in the dCA1 (Bliss and Collingridge, 1993; Lisman, 2017; Martin et al., 2000). However, more recent targeted genetic manipulation studies have shown that mice with dCA1-targeted knockout of NMDA receptor (NMDAR) subunit, NR1, have an intact formation of spatial and contextual fear memories (Bannerman et al., 2012; Hirsch et al., 2015). However, NMDAR-dependent synaptic transmission is required for spatial choice (Bannerman et al., 2012) and contextual fear extinction (Hirsch et al., 2015). Accordingly, it has been proposed that NMDAR-dependent plasticity in the dCA1 has a crucial role in detecting and resolving contradictory or ambiguous memories when spatial information is required (Bannerman et al., 2014). For example, dCA1 NMDAR-dependent plasticity would be required during extinction training of contextual fear memories, in which an animal recalls aversive memories of the context (or cues) and experiences a conflicting new experience of the same context being safe. In agreement with this hypothesis, a global loss-of-function of PSD-95, which impacts NMDAR-dependent synaptic plasticity, impairs extinction, but not cued fear memory formation (Fitzgerald et al., 2015). Our experiments are the first to show that dCA1-targeted genetic manipulation blocking the phosphorylation of PSD-95 at serine 73, prevents activity-induced synaptic remodeling and strengthening required for the updating of partly extinguished fear memories. Thus, our data support the hypothesis that PSD-95-dependnet synaptic plasticity of the dCA1 is necessary to resolve contradictory information about the context.

Interestingly, extinction-induced and PSD-95-driven synaptic plasticity of dCA1 does not impair the initial encoding of fear extinction memory but rather prevents the updating of a partly extinguished contextual fear memory. Thus, the PSD-95-dependent synaptic plasticity in the dCA1 observed after the initial memory extinction session maintains the circuit's propensity for contextual memory updating rather than drive or encode updated memories. In agreement with this hypothesis, temporary chemogenetic inhibition of dCA1 or overexpression of phosphorylation deficient PSD-95 protein during contextual fear extinction memory prevents extinction-induced expression of PSD-95 and future updating of the contextual fear memory. We also show that the dCA1 inhibition, specifically during the first extinction session, impairs the updating of contextual fear memory.

Our data indicate that the extinction of contextual fear induces the upregulation of PSD-95 expression in the stOri and stLM, while the protein levels in stRad are not changed. These alterations are accompanied by the increased median area of PSDs, indicating synapse remodeling in the distal strata of dendrites. This synaptic change pattern is strikingly different from the changes observed immediately after contextual fear memory encoding, as synaptic remodeling is observed in the stRad (Radwanska et al., 2011). These observations support the idea that different CA1 inputs are involved in memory formation and updating. CA3 neurons project to the stRad and stOri regions of CA1 pyramidal neurons, the nucleus reuniens (Re) projects to the stOri and stLM, and the entorhinal cortex (EC) projects to the stLM (Hoover

and Vertes, 2012; Ishizuka et al., 1990; Kajiwara et al., 2008; Vertes, 2015). Thus, the pattern of synaptic changes induced by contextual fear extinction co-localises with the domains innervated by the Re and EC, suggesting that these inputs are regulated during contextual fear extinction. In agreement with our observations, previous data showed that the EC is activated during and is required for contextual fear extinction memory in animal models (Baldi and Bucherelli, 2014; Bevilaqua et al., 2006). Human studies also showed that EC-CA1 projections are activated by cognitive prediction error (that may drive memory updating or extinction), while CA3-CA1 projections are activated by memory recall without prediction errors (Bein et al., 2020). The role of the Re in fear memory encoding, retrieval, extinction and generalisation has been demonstrated (Ramanathan et al., 2018; Troyner and Jose Bertoglio, 2020; Xu and Südhof, 2013). Still, it has to be established whether the plasticity of dCA1 synapses is specific to Re and/or EC projections.

PSD-95 affects the structure and function of glutamatergic synapses. In particular, *in vitro* studies showed PSD-95 overexpression increases the size of glutamatergic synapses (Nikonenko et al., 2008). Our study is the first to show how overexpression of PSD-95 and PSD-95 serine 73 phosphorylation influence dCA1 glutamatergic synapses *in vivo*. We confirm that the overexpression of native and phosphorylation-deficient PSD-95 increases the median areas of PSDs, and it also results in a loss of small dendritic spines. Thus, the structural consequences of PSD-95 overexpression *in vivo* are profound as they involve the global remodeling of the local circuit. The long-term elimination and up-scaling of synapses are not regulated by PSD-95 serine 73 phosphorylation. Moreover, we demonstrate that contextual fear extinction induces rapid loss of synapses in the stOri that is accompanied by heterosynaptic upregulation of PSD-95 levels, growth of the synapses and increased synaptic transmission. These changes agree with studies demonstrating an upregulation of PSD-95 levels during memory formation and recall in the hippocampus and cortex, respectively (Elkobi et al., 2008; Zanca et al., 2019).

Moreover, these synaptic processes allude to the Hebbian strengthening of activated synapses and heterosynaptic weakening of adjacent synapses observed in activated visual cortex neurons and *in vitro* (El-Boustani et al., 2018; Royer and Paré, 2003). This study is the first description of bidirectional plasticity of dendritic spines in the dCA1 during attenuation of fear memories. Previously, the heterosynaptic weakening was shown to be driven by the expression of CaMKII-regulated Arc protein (El-Boustani et al., 2018). Here, we show that both aspects of the synaptic process are coordinated by CaMKII-dependent phosphorylation of PSD-95 at serine 73 (Gardoni et al., 2006). This is a new function of PSD-95 serine 73 as previously it was shown to negatively regulate activity-induced spine growth (Steiner et al., 2008). The functional meaning of the elimination vs. growth of the synapses during contextual fear extinction still remains unclear. A possible explanation is that synaptic elimination promotes the weakening of the original memory trace, while synaptic growth updates a contextual fear memory towards safety. This hypothesis, however, needs to be validated in future experiments. In particular, it would be interesting to see whether the elimination and growth of synapses are projection-specific.

Conclusions

Our study pinpoints a cellular mechanism that operates in the dCA1 area and contributes to contextual fear memory attenuation. We propose that the propensity for updating of contextual fear memories relies on opposing synaptic processes that both require PSD-95 serine 73 phosphorylation: strengthening of synapses and rapid elimination of small dendritic spines. Since new or long-lasting memories may be repeatedly reorganized upon

recall (Nader et al., 2000; Schafe et al., 2001), the molecular and cellular mechanisms involved in updating the existing memories provide excellent targets for fear memory impairment therapies. In particular, understanding the mechanisms that underlie contextual fear extinction may be relevant for post-traumatic stress disorder treatment.

Acknowledgments, Funding and Disclosure

This work was supported by a National Science Centre (Poland) Grant No. 2015/19/B/NZ4/02996 and 2013/08/W/NZ4/00861 to KR. PRELUDIUM Grant No. 2016/21/N/NZ4/03304 to MZ and PRELUDIUM Grant No. 2015/19/N/NZ4/03611 to KŁ. TW was supported by National Science Centre (Poland) (Grant No. 2017/26/E/NZ4/00637). The project was carried out using CePT infrastructure financed by the European Union - The European Regional Development Fund within the Operational Program "Innovative economy" for 2007-2013.

MZ, MB, KFT and KR designed the experiments; MZ, MB, MNS, MR, AN, AC, KTF, AS, KŁ, TW and MŚ performed the experiments; MZ, MB, ES, MŚ, MR, KŁ, KFT, TB, JW and KR analyzed data. MZ, MB and KR drafted the manuscript. All authors had critical input to the final version of the manuscript. Authors report no financial interests or conflicts of interest.

Light and microscopy experiments were performed at the Laboratory of Imaging Tissue Structure and Functions.

MATERIALS AND METHODS

A full description of Materials and Methods are available in supplementary material online.

Animals

C57BL/6J and Thy1-GFP(M) (Feng et al., 2009b) mice were used in the experiments. The experiments were undertaken in accordance with the Animal Protection Act of Poland and approved by the I Local Ethics Committee (261/2012, Warsaw, Poland).

Contextual fear conditioning

The animals were trained in a conditioning chamber (Med Associates Inc, St Albans, USA) in a soundproof box. Mice were placed in the training chamber, and after a 148 s introductory period, a foot shock (2 s, 0.7 mA) was presented. The shock was repeated 5 times at 90 s inter-trial intervals. Contextual fear memory was tested and extinguished 24 h after training by re-exposing mice to the conditioning chamber for 30 minutes without US presentation, followed by a second 30-minute extinction session the following day. Freezing and locomotor activity of mice was automatically scored. The experimenters were blind to the experimental groups.

REFERENCES

Abraham, W.C., Jones, O.D., and Glanzman, D.L. (2019). Is plasticity of synapses the mechanism of long-term memory storage? Npj Sci. Learn. *4*.

Attardo, A., Fitzgerald, J.E., and Schnitzer, M.J. (2015). Impermanence of dendritic spines in live adult CA1 hippocampus. Nature *523*, 592–596.

Aziz, W., Kraev, I., Mizuno, K., Kirby, A., Fang, T., Rupawala, H., Kasbi, K., Rothe, S., Jozsa, F., Rosenblum, K., et al. (2019). Multi-input Synapses, but Not LTP-Strengthened Synapses, Correlate with Hippocampal Memory Storage in Aged Mice. Curr. Biol. *29*, 3600–3610.

Baldi, E., and Bucherelli, C. (2014). Entorhinal cortex contribution to contextual fear conditioning extinction and reconsolidation in rats. Neurobiol. Learn. Mem. *110*, 64–71.

Baldi, E., and Bucherelli, C. (2015). Brain sites involved in fear memory reconsolidation and extinction of rodents. Neurosci. Biobehav. Rev. *53*, 160–190.

Bannerman, D.M., Bus, T., Taylor, A., Sanderson, D.J., Schwarz, I., Jensen, V., Hvalby, Ø., Rawlins, J.N.P., Seeburg, P.H., and Sprengel, R. (2012). Dissecting spatial knowledge from spatial choice by hippocampal NMDA receptor deletion. Nat. Neurosci. *15*, 1153–1159.

Bannerman, D.M., Sprengel, R., Sanderson, D.J., Mchugh, S.B., Rawlins, J.N.P., Monyer, H., and Seeburg, P.H. (2014). Hippocampal synaptic plasticity, spatial memory and anxiety. Nat. Rev. Neurosci. *15*, 181–192.

Bats, C., Groc, L., and Choquet, D. (2007). The Interaction between Stargazin and PSD-95 Regulates AMPA Receptor Surface Trafficking. Neuron *53*, 719–734.

Bein, O., Duncan, K., and Davachi, L. (2020). Mnemonic prediction errors bias hippocampal states. Nat. Commun. *11*.

Béïque, J.C., and Andrade, R. (2003). PSD-95 regulates synaptic transmission and plasticity in rat cerebral cortex. J. Physiol. *546*, 859–867.

Bevilaqua, L.R., Bonini, J.S., Rossato, J.I., Izquierdo, L.A., Cammarota, M., and Izquierdo, I. (2006). The entorhinal cortex plays a role in extinction. Neurobiol. Learn. Mem. *85*, 192–197.

Bishop, D., Nikić, I., Brinkoetter, M., Knecht, S., Potz, S., Kerschensteiner, M., and Misgeld, T. (2011). Near-infrared branding efficiently correlates light and electron microscopy. Nat. Methods *8*, 568–570.

Bliss, T.V.P., and Collingridge, G.L. (1993). A synaptic model of memory: Long-term potentiation in the hippocampus. Nature *361*, 31–39.

Chen, X., Nelson, C.D., Li, X., Winters, C.A., Azzam, R., Sousa, A.A., Leapman, R.D., Gainer, H., Sheng, M., and Reese, T.S. (2011). PSD-95 is required to sustain the molecular organization of the postsynaptic density. J. Neurosci. *31*, 6329–6338.

Cheng, D. (2006). Relative and Absolute Quantification of Postsynaptic Density Proteome Isolated from Rat Forebrain and Cerebellum*. Mol. Cell. Proteomics 1158–1170.

Chetkovich, D.M., Chen, L., Stocker, T.J., Nicoll, R.A., and Bredt, D.S. (2002). Phosphorylation of the postsynaptic density-95 (PSD-95)/discs large/zona occludens-1 binding site of stargazin regulates binding to PSD-95 and synaptic targeting of AMPA receptors. J. Neurosci. *22*, 5791–5796.

Deerinck, T.J., Bushong, E. a., Thor, a., and Ellisman, M.H. (2010). NCMIR methods for 3D

EM: A new protocol for preparation of biological specimens for serial block face scanning electron microscopy. Microscopy 6–8.

Denk, W., and Horstmann, H. (2004). Serial block-face scanning electron microscopy to reconstruct three-dimensional tissue nanostructure. PLoS Biol. *2*, e329.

Ehrlich, I., and Malinow, R. (2004). Postsynaptic Density 95 controls AMPA Receptor Incorporation during Long-Term Potentiation and Experience-Driven Synaptic Plasticity. J. Neurosci. *24*, 916–927.

Ehrlich, I., Klein, M., Rumpel, S., and Malinow, R. (2007). PSD-95 is required for activity-driven synapse stabilization. Proc. Natl. Acad. Sci. U. S. A. *104*, 4176–4181.

El-Boustani, S., Ip, J.P.K., Breton-Provencher, V., Knott, G.W., Okuno, H., Bito, H., and Sur, M. (2018). Locally coordinated synaptic plasticity of visual cortex neurons in vivo. Science (80-.). *360*, 1349–1354.

El-Husseini, A.E., Schnell, E., Chetkovich, D.M., Nicoll, R.A., and Bredt, D.S. (2000). PSD-95 involvement in maturation of excitatory synapses. Science *290*, 1364–1368.

Elkobi, A., Ehrlich, I., Belelovsky, K., Barki-Harrington, L., and Rosenblum, K. (2008). ERK-dependent PSD-95 induction in the gustatory cortex is necessary for taste learning, but not retrieval. Nat. Neurosci. *11*, 1149–1151.

Feng, G., Mellor, R.H., Bernstein, M., Keller-Peck, C., Nguyen, Q.T., Wallace, M., Nerbonne, J.M., Lichtman, J.W., and Sanes, J.R. (2000). Imaging neuronal subsets in transgenic mice expressing multiple spectral variants of GFP. Neuron *28*, 41–51.

Fitzgerald, P.J., Pinard, C.R., Camp, M.C., Feyder, M., Sah, A., Bergstrom, H.C., Graybeal, C., Liu, Y., Schlüter, O.M., Grant, S.G., et al. (2015). Durable fear memories require PSD-95. Mol. Psychiatry *20*, 901–912.

Frankland, P.W., and Bontempi, B. (2005). The organization of recent and remote memories. Nat. Rev. Neurosci. *6*, 119–130.

Gardoni, F., Polli, F., Cattabeni, F., and Di Luca, M. (2006). Calcium-calmodulin-dependent protein kinase II phosphorylation modulates PSD-95 binding to NMDA receptors. Eur. J. Neurosci. *24*, 2694–2704.

Garín-Aguilar, M.E., Díaz-Cintra, S., Quirarte, G.L., Aguilar-Vázquez, A., Medina, A.C., and Prado-Alcalá, R.A. (2012). Extinction procedure induces pruning of dendritic spines in CA1 hippocampal field depending on strength of training in rats. Front. Behav. Neurosci. *6*, 1–6.

Hirsch, S.J., Regmi, N.L., Birnbaum, S.G., and Greene, R.W. (2015). CA1-specific deletion of NMDA receptors induces abnormal renewal of a learned fear response. Hippocampus *25*, 1374–1379.

Hoover, W.B., and Vertes, R.P. (2012). Collateral projections from nucleus reuniens of thalamus to hippocampus and medial prefrontal cortex in the rat: A single and double retrograde fluorescent labeling study. Brain Struct. Funct. *217*, 191–209.

Hughes, L., Hawes, C., Monteith, S., and Vaughan, S. (2014). Serial block face scanning electron microscopy-the future of cell ultrastructure imaging. Protoplasma *251*, 395–401.

Ishizuka, N., Weber, J., and Amaral, D.G. (1990). Organization of intrahippocampal projections originating from CA3 pyramidal cells in the rat. J. Comp. Neurol. *295*, 580–623.

Kajiwara, R., Wouterlood, F.G., Sah, A., Boekel, A.J., Baks-Te Bulte, L.T.G., and Witter, M.P. (2008). Convergence of entorhinal and CA3 inputs onto pyramidal neurons and interneurons in hippocampal area CA1 - An anatomical study in the rat. Hippocampus *18*, 266–280.

Knott, G.W., Holtmaat, A., Trachtenberg, J.T., Svoboda, K., and Welker, E. (2009). A protocol for preparing GFP-labeled neurons previously imaged in vivo and in slice preparations for light and electron microscopic analysis. Nat. Protoc. *4*, 1145–1156.

Kornau, H., Schenker, L., Kennedy, M., and Seeburg, P. (1995). Domain interaction between NMDA receptor subunits and the postsynaptic density protein PSD-95. Science (80-.). *269*, 1737–1740.

Lee, H.M., Giguere, P.M., and Roth, B.L. (2014). DREADDs: Novel tools for drug discovery and development. Drug Discov. Today *19*, 469–473.

Lisman, J. (2017). Criteria for identifying the molecular basis of the engram (CaMKII, PKMzeta). Mol. Brain *10*, 1–10.

Mahmmoud, R.R., Sase, S., Aher, Y.D., Sase, A., Gröger, M., Mokhtar, M., Höger, H., and Lubec, G. (2015). Spatial and working memory is linked to spine density and mushroom spines. PLoS One *10*, 1–15.

Martin, S.J., Grimwood, P.D., and Morris, R.G.M. (2000). Synaptic Plasticity and Menory. Ann.Rev.Neurosci 649–711.

Migaud, M., Charlesworth, P., Dempster, M., Webster, L.C., Watabe, A.M., Makhinson, M., He, Y., Ramsay, M.F., Morris, R.G., Morrison, J.H., et al. (1998). Enhanced long-term potentiation and impaired learning in mice with mutant postsynaptic density-95 protein. Nature *396*, 433–439.

Morris, R.G.M., Moser, E.I., Riedel, G., Martin, S.J., Sandin, J., Day, M., and O'Carroll, C. (2003). Elements of a neurobiological theory of the hippocampus: The role of activity-dependent synaptic plasticity in memory. Philos. Trans. R. Soc. B Biol. Sci. *358*, 773–786.

Nader, K., Schafe, G.E., and Le Doux, J.E. (2000). Fear memories require protein synthesis in the amygdala for reconsolidation after retrieval. Nature *406*, 722–726.

Neves, G., Cooke, S.F., and Bliss, T.V.P. (2008). Synaptic plasticity, memory and the hippocampus: A neural network approach to causality. Nat. Rev. Neurosci. *9*, 65–75.

Nikonenko, I., Boda, B., Steen, S., Knott, G., Welker, E., and Muller, D. (2008). PSD-95 promotes synaptogenesis and multiinnervated spine formation through nitric oxide signaling. J. Cell Biol. *183*, 1115–1127.

Radwanska, K., Medvedev, N.I., Pereira, G.S., Engmann, O., Thiede, N., Moraes, M.F.D., Villers, A., Irvine, E.E.E.E.E., Maunganidze, N.S.N.S.N.S., Pyza, E.M.E.M.E.M.E.M.E.M., et al. (2011). Mechanism for long-term memory formation when synaptic strengthening is impaired. Proc. Natl. Acad. Sci. U. S. A. *108*, 18471–18475.

Ramanathan, K.R., Ressler, R.L., Jin, J., and Maren, S. (2018). Nucleus reuniens is required

for encoding and retrieving precise, hippocampal-dependent contextual fear memories in rats. J. Neurosci. *38*, 9925–9933.

Restivo, L., Vetere, G., Bontempi, B., and Ammassari-Teule, M. (2009). The formation of recent and remote memory is associated with time-dependent formation of dendritic spines in the hippocampus and anterior cingulate cortex. J. Neurosci. *29*, 8206–8214.

van Rooij, S.J.H., Stevens, J.S., Ely, T.D., Hinrichs, R., Michopoulos, V., Winters, S.J., Ogbonmwan, Y.E., Shin, J., Nugent, N.R., Hudak, L.A., et al. (2018). The Role of the Hippocampus in Predicting Future Posttraumatic Stress Disorder Symptoms in Recently Traumatized Civilians. Biol. Psychiatry *84*, 106–115.

Royer, S., and Paré, D. (2003). Conservation of total synaptic weight through balanced synaptic depression and potentiation. Nature *422*, 518–522.

Schafe, G.E., Nader, K., Blair, H.T., and Ledoux, J.E. (2001). Memory consolidation of Pavlovian fear conditioning: a cellular and molecular perspective. Trends Neurosci. *24*, 540–546.

Schnell, E., Sizemore, M., Karimzadegan, S., Chen, L., Bredt, D.S., and Nicoll, R.A. (2002). Direct interactions between PSD-95 and stargazin control synaptic AMPA receptor number. Proc. Natl. Acad. Sci.

Schuette, P.J., Reis, F.M.C.V., Maesta-Pereira, S., Chakerian, M., Torossian, A., Blair, G., Wang, W., Blair, H.T., Fanselow, M.S., Kao, J.C., et al. (2020). Long-term characterization of hippocampal remapping during contextual fear acquisition and extinction. J. Neurosci. JN-RM-1022-20.

Stansley, B.J., Fisher, N.M., Gogliotti, R.G., Lindsley, C.W., Conn, P.J., and Niswender, C.M. (2018). Contextual fear extinction induces hippocampal metaplasticity mediated by metabotropic glutamate receptor 5. Cereb. Cortex *28*, 4291–4304.

Stein, V., House, D.R.C., Bredt, D.S., and Nicoll, R.A. (2003). Postsynaptic density-95 mimics and occludes hippocampal long-term potentiation and enhances long-term depression. J. Neurosci. *23*, 5503–5506.

Steiner, P., Higley, M.J., Xu, W., Czervionke, B.L., Malenka, R.C., and Sabatini, B.L. (2008). Destabilization of the Postsynaptic Density by PSD-95 Serine 73 Phosphorylation Inhibits Spine Growth and Synaptic Plasticity. Neuron *60*, 788–802.

Strange, B.A., Witter, M.P., Lein, E.S., and Moser, E.I. (2014). Functional organization of the hippocampal longitudinal axis. Nat. Rev. Neurosci. *15*, 655–669.

Sturgill, J.F., Steiner, P., Czervionke, B.L., and Sabatini, B.L. (2009). Distinct Domains within PSD-95 Mediate Synaptic Incorporation, Stabilization, and Activity-Dependent Trafficking. J. Neurosci. *29*, 12845–12854.

Taft, C.E., and Turrigiano, G.G. (2014). PSD-95 promotes the stabilization of young synaptic contacts. Philos. Trans. R. Soc. B Biol. Sci. *369*.

Troyner, F., and Jose Bertoglio, L. (2020). Thalamic nucleus reuniens regulates fear memory destabilization upon retrieval. Neurobiol. Learn. Mem. *175*, 107313.

Vertes, R.P. (2015). Major diencephalic inputs to the hippocampus: Supramammillary

nucleus and nucleus reuniens. Circuitry and function (Elsevier B.V.).

Xu, W., and Südhof, T.C. (2013). A neural circuit for memory specificity and generalization. Science (80-.). *339*, 1290–1295.

Zanca, R.M., Sanay, S., Avila, J.A., Rodriguez, E., Shair, H.N., and Serrano, P.A. (2019). Contextual fear memory modulates PSD95 phosphorylation, AMPAr subunits, PKMζ and PI3K differentially between adult and juvenile rats. Neurobiol. Stress *10*.

Supplementary Materials

Authors: Magdalena Ziółkowska[&,1], Malgorzata Borczyk[&,1,2], Agata Nowacka[1], Maria Nalberczak-Skóra[1], Małgorzata Alicja Śliwińska[1,3], Magdalena Robacha[1], Kacper Łukasiewicz[1], Anna Cały[1], Edyta Skonieczna[1], Kamil F. Tomaszewski[1], Tomasz Wójtowicz[4], Jakub Włodarczyk[4], Tytus Bernaś[3,5], Ahmad Salamian[1] and Kasia Radwanska[1*].

[1]Laboratory of Molecular Basis of Behavior, the Nencki Institute of Experimental Biology of Polish Academy of Sciences.

[2]Department Molecular Neuropharmacology, Maj Institute of Pharmacology of Polish of Academy of Sciences, Warsaw, Poland

[3]Laboratory of Imaging Tissue Structure and Function, The Nencki Institute of Experimental Biology of Polish Academy of Sciences, Warsaw, Poland.

[4]Laboratory of Cell Biophysics, the Nencki Institute of Experimental Biology of Polish Academy of Sciences.

[5]Department of Anatomy and Neurology, VCU School of Medicine, 1101 East Marshall Street, Richmond, Virginia 23298

[&]equal contribution.

*Corresponding author: Kasia Radwanska, Ph.D., Laboratory of Molecular Basis of Behavior, Nencki Institute of Experimental Biology of Polish Academy of Sciences, ul. L. Pasteura 3, Warsaw 02-093, Poland; e-mail: k.radwanska@nencki.edu.pl; tel: +48501736942

SUPPLEMENTARY RESULTS

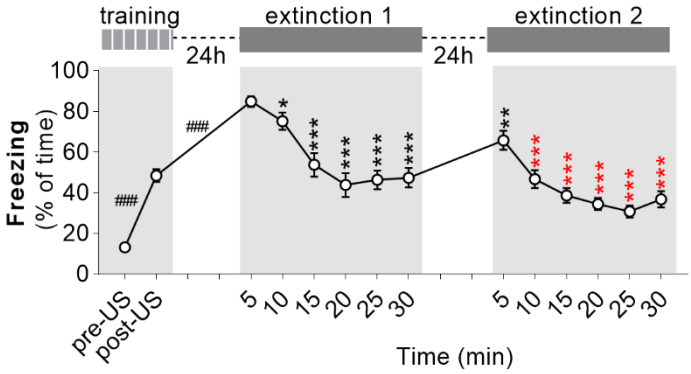

Supplementary Figure 1. Experimental timeline and the freezing levels of the mice during contextual fear conditioning training and two fear extinction sessions. C57BL/6j mice (n = 15) showed low freezing levels in a novel context before delivery of electric shocks (pre-US) and freezing increased during the training (post-US) ($t = 14.91$, $df = 14$, $^{###}P < 0.001$), indicating fear memory formation. Twenty-four hours later, the animals were re-exposed to the training context without US presentation for the first fear extinction memory session (extinction 1). Freezing levels were high at the beginning of the session, indicating fear memory retrieval and decreased within the session (RM ANOVA with Holm-Sidak's multiple comparisons tests (black asterisks), $F(3.011, 42.15) = 20.72$, $P < 0.001$) indicating the formation of fear memory extinction. Next, we tested the consolidation of fear extinction memory 24 hours later (extinction 2). At the beginning of extinction 2, the freezing levels were lower than at the beginning of extinction 1 ($t = 3.843$, $df = 14$, $^{**}P = 0.0018$), indicating that the formation of long-term fear extinction memory. Moreover, the freezing levels further decreased during extinction 2 (RM ANOVA with Holm-Sidak's multiple comparisons tests (red asterisks, $F(2.410, 33.74) = 17$, $P < 0.001$), indicating further updating of contextual fear memory.

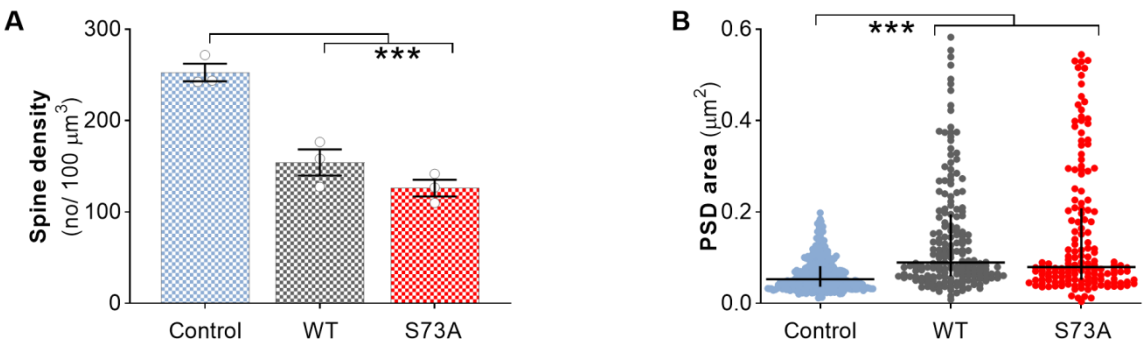

Supplementary Figure 2. Overexpression of PSD-95 (WT and S73A) in dCA1 reduces dendritic spine density and increases PSDs size. Mice were stereotactically injected with AAVs encoding Control (mCherry), PSD-95 WT or S73A in the dCA1 and trained in contextual fear memory conditioning and extinction. (**A**) Mean density of dendritic spines was downregulated after overexpression of WT and S73A, compared to Control mice (One-way ANOVA, $F(2, 6) = 34.59$, $^{***}P < 0.001$). (**B**) Median size of PSDs was increased after overexpression of WT and S73A, compared to Control mice (Kruskal-Wallis statistic, $H = 108.9$, $^{***}P < 0.001$).

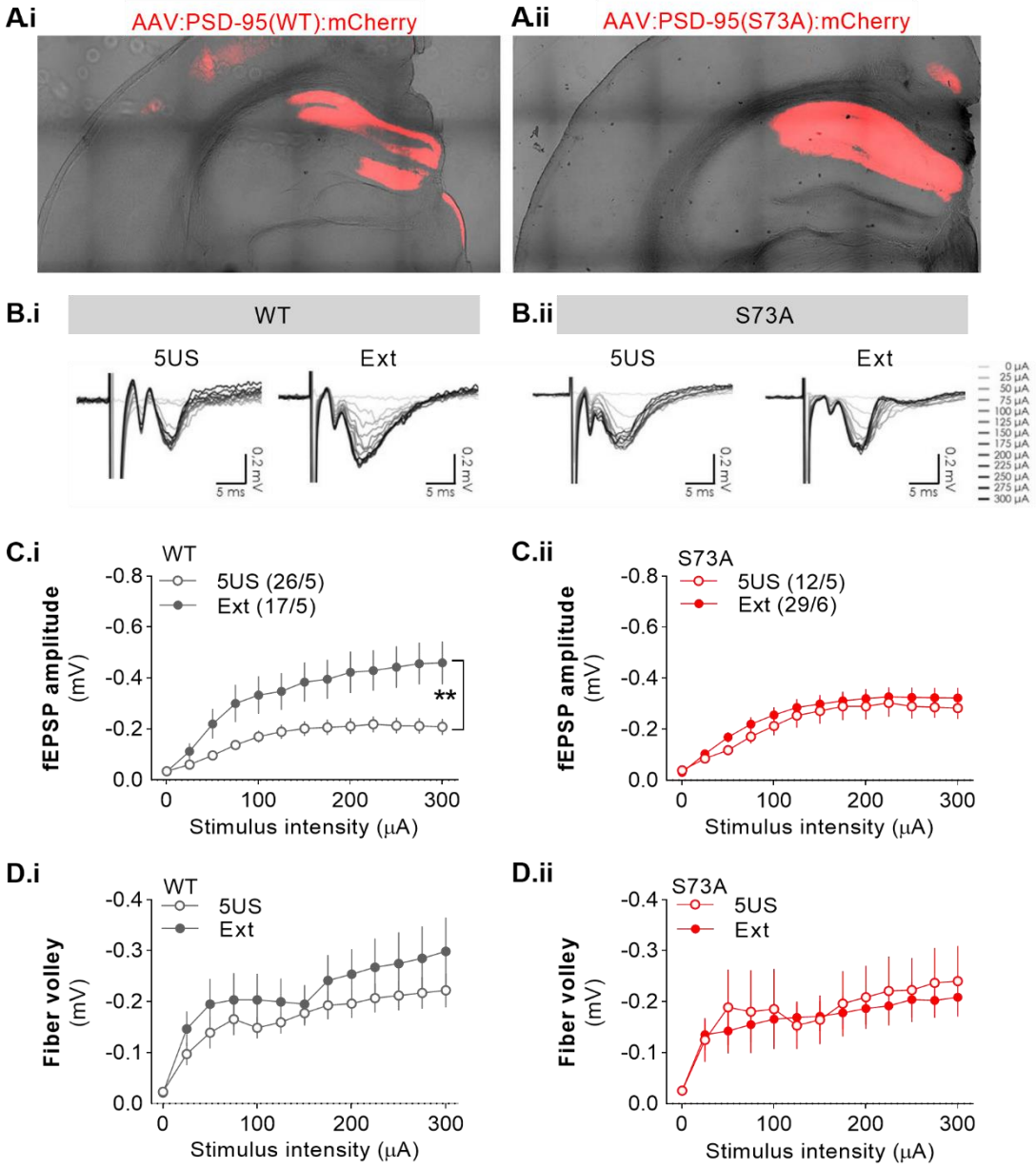

Supplementary Figure 3. Phosphorylation of PSD-95 at S73 is required for fEPSP changes in stOri after fear extinction training. Mice were injected with PSD-95 WT or S73A in dCA1. Field excitatory postsynaptic potentials (fEPSPs) were recorded in stOri of dCA1 in response to the stimulation from the Schaffer collaterals. Moreover, the population spikes in the stratum pyramidale and fiber volleys were recorded and measured. **(A)** Microphotographs of PSD-95 WT and S73A expression in the CA1. **(B)** Representative fEPSPs evoked by stimuli of different intensities in stOri of the mice expressing PSD-95 WT and S73A respectively and sacrificed before or after fear extinction training. **(C)** Input–output plot for stimulus intensity versus fEPSP amplitude recorded in response to increasing intensities of stimulation in stOri. The fEPSP amplitudes were affected by the extinction training in the mice expressing **(i)** WT (RM ANOVA, $F(1, 42) = 7.581$, $^{**}P = 0.0087$), **(ii)** but not S73A ($F(1, 36) = 0.404$, $P = 0.528$). (**D**) Input–output functions for stimulus intensity versus fiber volley recorded in response to increasing intensities of stimulation. No effect of contextual fear extinction was observed in mice expressing **(i)** WT ($F(1, 30) = 0.080$, $P = 0.778$) or **(ii)** S73A ($F(1, 30) = 0.080$, $P = 0.778$). The numbers of the analysed sections/mice per experimental group are indicated in (C).

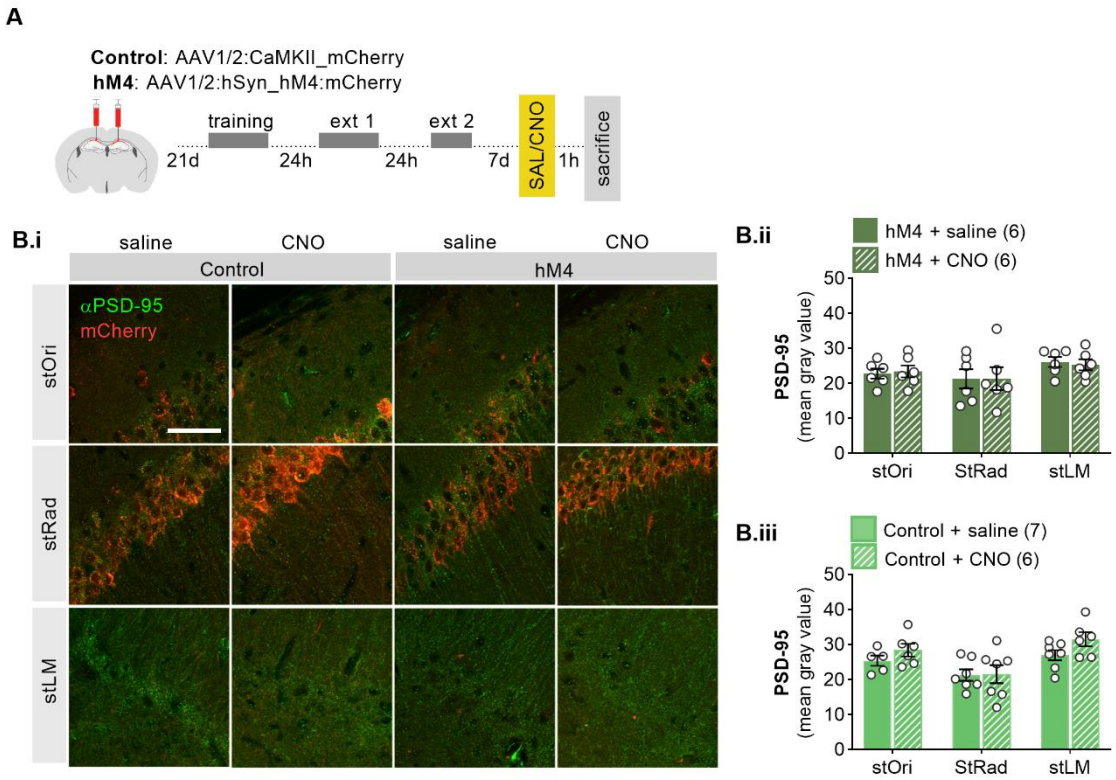

Supplementary Figure 4. Chemogenetic inhibition of dCA1 after training does not affect PSD-95 expression. (A) Experimental timeline during fear conditioning and fear extinction sessions (ext1 and ext2) of the mice with Control and hM4 virus. Mice were trained three weeks after the surgery and virus expression. In all groups, saline or CNO (1 mg/kg) was systemically injected 7 days after the ext2. Mice were sacrificed 60 minutes after the injection. Behavioral data are shown in Fig. 2. **(B) (i)** Representative, confocal scans of the brain slices immunostained for PSD-95. Scale bar, 10 μm. (**ii-iii)** Summary of data quantifying the expression of PSD-95 in three domains of dCA1 in mice with Control or hM4 virus. No effect of the drug was observed in any of the virus groups (RM ANOVA, Control: $F(1, 12) = 1.823$, $P = 0.322$; hM4: $F(1, 10) = 0.0003$, $P = 0.988$). The numbers of mice per experimental group are in the legends (**B.ii-iii**).

SUPPLEMENTARY MATERIALS AND METHODS

Animals

C57BL/6J male mice were purchased from Białystok University, Poland. Thy1-GFP(M) (The Jackson Laboratory, JAX:007788, RRID:IMSR_JAX:007788) mutant mice were bred as heterozygotes at Nencki Institute, and PCR genotyped as previously described (Feng et al., 2000). All mice in the experiments were 7-9-week old. The mice were housed in groups of two to six and maintained on a 12 h light/dark cycle with food and water ad libitum. All experiments with transgenic mice used approximately equal numbers of males and females. The experiments were undertaken according to the Animal Protection Act of Poland and approved by the I Local Ethics Committee (261/2012, Warsaw, Poland).

Contextual fear conditioning

The animals were trained in a conditioning chamber (Med Associates Inc, St Albans, USA) in a soundproof box. The chamber floor had a stainless steel grid for shock delivery. Before training, the chamber was cleaned with 70% ethanol, and a paper towel soaked in ethanol was placed under the grid floor. To camouflage background noise in the behavioral room, a white noise generator was placed inside the soundproof box.

On the conditioning day, the mice were brought from the housing room into a holding room to acclimatize for 30 min before training. Next, mice were placed in the training chamber, and after a 148 s introductory period, a foot shock (2 s, 0.7 mA) was presented. The shock was repeated 5 times, at 90 s inter-trial intervals. Thirty seconds after the last shock, the mouse was returned to its home cage. Contextual fear memory was tested and extinguished 24 h after training by re-exposing mice to the conditioning chamber for 30 minutes without US presentation, followed by the second 30-minute extinction session on the following day. A video camera was fixed inside the door of the sound attenuating box for the behavior to be recorded and scored. Freezing behavior (defined as complete lack of movement, except respiration) and locomotor activity of mice were automatically scored. The experimenters were blind to the experimental groups.

CNO administration. Clozapine N-Oxide (CNO) was dissolved in 0.9% saline. One or 3 mg/kg CNO was intraperitoneally (i.p.) injected 30 min before the behavioral extinction session. These doses of CNO did not induce any overt abnormal behaviors except for those reported in the study.

Immunostaining

Mice were anesthetized and perfused with cold phosphate buffer pH 7.4, followed by 0.5% 4% PFA in phosphate buffer. Brains were removed and postfixed o/n in 4°C. Brains were kept in 30% sucrose in PBS for 72h. Coronal brain sections were prepared using cryosectioning (40 µm thick, Cryostat CM1950, Leica Biosystems Nussloch GmbH, Wetzlar, Germany) and stored in a cryoprotecting solution in –20°C (PBS, 15% sucrose (Sigma-Aldrich), 30% ethylene glycol (Sigma-Aldrich), and 0.05% NaN_3 (SigmaAldrich). Before staining, sections were washed 3 × PBS and blocked for 1 hour at room temperature (RT) in 5% NDS with 0.3% Triton X-100 in PBS and then incubated o/n, 4°C with PSD-95 primary antibodies (1:500, Millipore, MAB1598, RRID:AB_11212185). On the second day slices were washed 3 × PBS with 0,3% Trition X-100 and incubated for 90 minutes with secondary antibodies conjugated with AlexaFluor 555 (1:500, Invitrogen, A31570, RRID:AB_2536180).

Slices were then mounted on microscope slides (Thermo Fisher Scientific) and covered with coverslips in Fluoromount-G medium with DAPI (00-4959-52, Invitrogen).

Confocal microscopy and image quantification

The microphotographs of dendritic spines in Thy1-GFP mice and fluorescent PSD-95 immunostaining were taken on a Spinning Disc confocal microscope (63 × oil objective, NA 1.4, pixel size 0.13 µm × 0.13 µm) (Zeiss, Göttingen, Germany). We took microphotographs (16 bit, z-stacks of 12-48 scans; 260 nm z-steps) of the dendrites from stratum oriens (stOri), stratum radiatum (stRad) and stratum lacunosum-moleculare (stLM) (6 dendrites per region per animal) of dorsal CA1 pyramidal neurons (AP, Bregma from -1.7 to 2.06). Each dendritic spine was manually outlined, and the spine area was measured with ImageJ 1.52n software measure tool. Custom-written Python scripts were used to analyze the mean gray value of PSD-95(+) puncta per dendritic spine.

The PSD-95 fluorescent immunostaining and PSD-95:mCherry over-expression were analyzed with Zeiss LSM 800 microscope equipped with Airy-Scan detection (63× oil objective and NA 1.4, pixel size 0.13 µm × 0.13 µm, 8 bit) (Zeiss, Göttingen, Germany). A series of 18 continuous optical sections (67.72 µm × 67.72 µm), at 0.26 µm intervals, were scanned along the z-axis of the tissue section. Six to eight z-stacks of microphotographs were taken per animal per region, from every sixth section through dCA1. Z-stacks were flattened to maximal projections and analyzed with Fiji software. Endogenious PSD-95 levels was assessed as an image mean gray value. Exogenious synaptic PSD-95:mCherry levels were measured by multiplying the number and size of the immunopositive synaptic-like puncta and than the total puncta area was divided by the area of the image and expressed as % area.

Stereotactic surgery

Mice were fixed in a stereotactic frame (51503, Stoelting, Wood Dale, IL, USA) and kept under isoflurane anesthesia (5% for induction, 1.5-2.0% during surgery). Adeno-associated viruses, serotype 1 and 2, (AAV1/2), solutions were injected into the dorsal CA1 area (Paxinos & Franklin 2001) at coordinates in relation to Bregma (AP, -2.1mm; ML, ±1.1 mm; DV, -1.3mm). 450 nl of AAV solutions were injected into the CA1 through a beveled 26 gauge metal needle, and 10 µl microsyringe (SGE010RNS, WPI, USA) connected to a pump (UMP3, WPI, Sarasota, USA), and its controller (Micro4, WPI, Sarasota, USA) at a rate 50 nl/ min. The needle was then left in place for 5 min, retracted +100 nm DV, and left for an additional 5 min to prevent unwanted spread of the AAV solution. Titers of AAV1/2 were: αCaMKII_PSD-95(WT):mCherry (PSD-95(WT)): 1.35 $x10^9$/µl, αCaMKII_PSD-95(S73A):mCherry (PSD-95(S73A)): 9.12 $x10^9$/µl), αCaMKII_mCherry (mCherry): viral titer 7.5 $x10^7$/µl (obtained from Karl Deisseroth's Lab), hSyn_HA-hM4D(Gi):mCherry (hM4) (Addgene plasmid #50475): 4.59 $x10^7$/µl. Mice were allowed to recover from anesthesia for 2-3 h on a heating pad and then transferred to individual cages where they stayed until complete skin healing, and next, they were returned to the home cages. The viruses were prepared at the Nencki Institute core facility, Laboratory of Animal Models. After training, the animals were perfused with 4% PFA in PBS and brain sections from the dorsal hippocampus were immunostained for PSD-95 and imaged with Zeiss Spinning Disc confocal microscope (magnification: 10x) to assess the extent of the viral expression and PSD-95 expression.

3D electron microscopy

Mice were transcardially perfused with cold phosphate buffer pH 7.4, followed by 0.5% EM-grade glutaraldehyde (G5882 Sigma-Aldrich) with 2% PFA in phosphate buffer pH

7.4 and postfixed overnight in the same solution. Brains were then taken out of the fixative and cut on a vibratome (Leica VT 1200) into 100 µm slices. Slices were kept in phosphate buffer pH 7.4, with 0.1% sodium azide in 4°C for up to 14 days. For AAV-injected animals, the fluorescence of exogenous proteins was confirmed in all slices by fluorescent imaging. Then, slices were washed 3 × in cold phosphate buffer and postfixed with a solution of 2% osmium tetroxide (#75632 Sigma-Aldrich) and 1.5 % potassium ferrocyanide (P3289 Sigma-Aldrich) in 0.1 M phosphate buffer pH 7.4 for 60 min on ice. Next, samples were rinsed 5 × 3 min with double distilled water (ddH_2O) and subsequently exposed to 1% aqueous thiocarbohydrazide (TCH) (#88535 Sigma) solution for 20 min. Samples were then washed 5 × 3 min with ddH_2O and stained with osmium tetroxide (1% osmium tetroxide in ddH_2O, without ferrocyanide) for 30 min in RT. Afterward, slices were rinsed 5 × 3 min with ddH_2O and incubated in 1% aqueous solution of uranium acetate overnight in 4°C. The next day, slices were rinsed 5 × 3 min with ddH_2O, incubated with lead aspartate solution (prepared by dissolving lead nitrate in L-aspartic acid as previously described (Deerinck et al., 2010)) for 30 min in 60°C and then washed 5 × 3 min with ddH_2O and dehydration was performed using graded dilutions of ice-cold ethanol (30%, 50%, 70%, 80%, 90%, and 2 × 100% ethanol, 5 min each). Then slices were infiltrated with Durcupan resin. A(17 g), B(17 g) and D(0,51 g) components of Durcupan (#44610 Sigma-Aldrich) were first mixed on a magnetic stirrer for 30 min and then 8 drops of DMP-30 (#45348 Sigma) accelerator were added (Knott et al., 2009). Part of the resin was then mixed 1:1 (v/v) with 100% ethanol and slices were incubated in this 50% resin on a clock-like stirrer for 30 min in RT. The resin was then replaced with 100% Durcupan for 1 hour in RT and then 100% Durcupan infiltration was performed o/n with constant slow mixing. The next day, samples were infiltrated with freshly prepared resin (as described above) for another 2 hours in RT, and then embedded between flat Aclar sheets (Ted Pella #10501-10). Samples were put in a laboratory oven for at least 48 hours at65°C for the resin to polymerize. After the resin hardened, the Aclar layers were separated from the resin embedded samples, dCA1 region was cut out with a razorblade. Caution was taken for the piece to contain minimal resin. Squares of approximately 1 × 1 × 1 mm were attached to aluminium pins (Gatan metal rivets, Oxford instruments) with very little amount of cyanacrylamide glue. After the glue dried, samples were mounted to the ultramicrotome to cut 1 µm thick slices. Slices were transferred on a microscope slide, briefly stained with 1% toluidine blue in 5% borate and observed under a light microscope to confirm the region of interest (ROI). Next, samples were grounded with silver paint (Ted Pella, 16062-15) and pinned for drying for 4 – 12 hours, before the specimens were mounted into the 3View2 chamber.

SBEM *imaging and 3D reconstructions*

Samples were imaged with Zeiss SigmaVP (Zeiss, Oberkochen, Germany) scanning electron microscope equipped with 3View2 chamber using a backscatter electron detector. Scans were taken in the middle portion of the CA1 stOri of the dorsal hippocampus. From each sample, 200 sections were collected (thickness 60 nm). Imaging settings: high vacuum with EHT 2.9-3.8 kV, aperture: 20 µm, pixel dwell time: 3 µs, pixel size: 5 – 6.2 nm. Scans were aligned using the ImageJ software (ImageJ -> Plugins -> Registration -> StackReg) and saved as .tiff image sequence. Next, alignment scans were imported to Reconstruct software (Fiala 2005), available at http://synapses.clm.utexas.edu/tools/reconstruct/reconstruct.stm (Synapse Web Reconstruct, RRID:SCR_002716). Spine density was analyzed from 3 bricks per animal with the unbiased brick method (Fiala and Harris 2001) per tissue volume. Brick dimensions 4.3 × 4.184 × 3 µm were chosen to exceed the length of the largest profiles in the data sets at least twice. To calculate the density of dendritic spines, the total volume of large tissue discontinuities was subtracted from the volume of the brick.

A structure was considered to be a dendritic spine when it was a definite protrusion from the dendrite, with electron-dense material (representing postsynaptic part of the synapse, PSD) on the part of the membrane that opposed an axonal bouton with at least 3 vesicles within a 50-nm distance from the cellular membrane facing the spine. For 3D reconstructions, PSDs and dendritic spines in one brick were reconstructed for each sample. PSDs were first reconstructed and second, their dendritic spines were outlined. To separate dendritic spine necks from the dendrites, a cut-off plane was used approximating where the dendritic surface would be without the dendritic spine. PSD volume was measured by outlining dark, electron-dense area on each PSD containing section. The PSD area was measured manually according to the Reconstruct manual. All non-synaptic protrusions were omitted in this analysis. For multi-synaptic spines, the PSD areas and volumes have been summed. In total, 1317 dendritic spines with their PSDs were manually segmented with the annotators blind to sample condition.

Correlative light-electron microscopy (CLEM)

CLEM workflow was based on a previously established protocol with some modifications (Bishop et al., 2011). Mice infused with PSD-95(WT) in the CA1 were perfused as described above. Brains were then removed and postfixed o/n in 4°C. 100 µm thick brain slices were cut on a vibratome and embedded in low melting point agarose in phosphate buffer and mounted into imaging chambers. mCherry fluorescence in the stRad was photographed using Zeiss LSM800, z-stacks of 60 images (60 µm thick) at 63 × magnification. Next, the slice was transferred under the 2P microscope (Zeiss MP PA Setup), where a Chameleon laser was used to brand mark the ROI (laser length 870 nm, laser power 85%, 250 scans of each line). Then, SBEM staining was performed as described above. The resin-embedded hippocampus was then divided into 4 rectangles and each was mounted onto metal pins to locate the laser-induced marks. SBEM scanned within the laser marked frame. The fluorescent image was overlaid onto the SBEM image using dendrites and cell nuclei as landmarks using ImageJ 1.48k software (RRID:SCR_003070).

Electrophysiology

Mice were deeply anesthesized with Isoflurane, decapitated and the brains were rapidly dissected and transfered into ice-cold cutting artificial cerebrospinal fluid (ACSF) consisting of (in mM): 87 NaCl, 2.5 KCl, 1.25 NaH2PO4, 25 NaHCO3, 0.5 CaCl2, 7 MgSO4, 20 D-glucose, 75 sacharose equilibrated with carbogen (5% CO2/95% O2). The brain was cut to two hemispheres and 350 µm thick coronal brain slices were cut in ice-cold cutting ACSF with Leica VT1000S vibratome. Slices were then incubated for 15 min in cutting ACSF at 32°C. Next the slices were transfered to recording ACSF containing (in mM): 125 NaCl, 2.5 KCl, 1.25 NaH_2PO_4, 25 $NaHCO_3$, 2.5 $CaCl_2$, 1.5 $MgSO_4$, 20 D-glucose equilibrated with carbogen and incubated for minimum 1 hour at room temperature (RT).

Extracellular field potential recordings were recorded in a submerged chamber perfused with recording ACSF in RT. The potentials were evoked with a Stimulus Isolator (A.M.P.I Isoflex) with a concentric bipolar electrode (FHC, CBARC75) placed in the stOri of CA2 on the experiment. The stimulating pulses were delivered at 0.1 Hz and the pulse duration was 0.3 ms. Recording electrodes (resistance 1-4 MΩ) were pulled from borosilicate glass (WPI, 1B120F-4) with a micropipette puller (Sutter Instruments, P-1000) and filled with recording ACSF. The recording electrodes were placed in stOri of dCA1. Simultaneously, a second recording electrode was placed in the stratum pyramidale to measure population spikes. For each slice, the recordings were done in stOri. Recordings were acquired with

MultiClamp 700B amplifier (Molecular Devices, California, USA), digitized with Digidata 1550B (Molecular Devices, California, USA) and pClamp 10.7 Clampex 10.0 software (Molecular Devices, California, USA). Input/output curves were obtained by increasing stimulation intensity by 25 μA in the range of 0-300 μA. All electrophysiological data was nalyzed with AxoGraph 1.7.4 software (Axon Instruments, U.S.A). The amplitude of fEPSP, relative amplitude of population spikes and fiber volley were measured.

Statistics

Data are presented as mean ± standard error of the mean (SEM) for populations with normal distribution or as median ± interquartile range (IQR) for populations with non-normal distribution. When the data met the assumptions of parametric statistical tests, results were analysed by one- or repeated measures two-way ANOVA, followed by Tukey's or Fisher's *post hoc* tests, where applicable. Data were tested for normality by using the Shapiro-Wilk test of normality and for homogeneity of variances by using the Levene's test. For repeated-measure data with missing observation, a linear mixed model was used to analyze the results, followed by pairwise comparisons with Sidak adjustment for multiple comparisons. Areas of dendritic spines and PSDs did not follow normal distributions and were analysed with the Kruskal-Wallis test. Frequency distributions of PSD area to the spine volume ratio were compared with the Kolmogorov-Smirnov test. Correlations were analysed using Spearman correlation (Spearman r (s_r) is shown), and the difference between slopes or elevation between linear regression lines was calculated with ANCOVA. Differences in means were considered statistically significant if $P < 0.05$. Analyses were performed using the Graphpad Prism 8 or Statistica software. Mice were excluded from the analysis only if they did not express the tested virus in the target region.